creative commons
COMMONS DEED

저작자표시-비영리-변경금지 2.0 대한민국

이용자는 아래의 조건을 따르는 경우에 한하여 자유롭게

- 이 저작물을 복제, 배포, 전송, 전시, 공연 및 방송할 수 있습니다.

다음과 같은 조건을 따라야 합니다:

저작자표시. 귀하는 원저작자를 표시하여야 합니다.

비영리. 귀하는 이 저작물을 영리 목적으로 이용할 수 없습니다.

변경금지. 귀하는 이 저작물을 개작, 변형 또는 가공할 수 없습니다.

- 귀하는, 이 저작물의 재이용이나 배포의 경우, 이 저작물에 적용된 이용허락조건을 명확하게 나타내어야 합니다.
- 저작권자로부터 별도의 허가를 받으면 이러한 조건들은 적용되지 않습니다.

저작권법에 따른 이용자의 권리는 위의 내용에 의하여 영향을 받지 않습니다.

이것은 이용허락규약(Legal Code)을 이해하기 쉽게 요약한 것입니다.

Disclaimer

dCollection

공학석사 학위논문

정적 전기장 문제에 대한 형상 최적화 설계

Shape design optimization

of electrostatic problems

2019년 08월

서울대학교 대학원

조선해양공학과

정 홍 연

정적 전기장 문제에 대한
형상 최적화 설계

Shape design optimization

of electrostatic problems

지도교수 조 선 호

이 논문을 공학석사 학위논문으로 제출함

2019년 7월

서울대학교 대학원

조선해양공학과

정 홍 연

정홍연의 공학석사 학위논문을 인준함

2019년 7월

위 원 장 홍 석 윤 (인)

부 위 원 장 조 선 호 (인)

위 원 이 신 형 (인)

초 록

전극에 의해 생성 된 전기장은 공학을 다룸에 있어 다양한 분야에 적용될 수 있다. 조선 해양 공학 분야에서는 선박 평형 수의 소독 과정에서 이용되는 전처리 장치를 하나의 예로 생각할 수 있다. 전처리 장치가 이용되는 연구 배경으로는 최근에 발효된 IMO 규정이 그 원인이다. 새로 발효된 IMO 규정은 해양에 배출되는 밸러스트 수의 품질에 대한 규제를 더욱 엄격하게 만들었다. 따라서, 밸러스트 수를 간단하고 효과적으로 살균 할 수 있는 방법에 대한 연구가 전 세계적으로 활발히 진행되고 있다. 본 연구는 그 중 하나의 방법인 전처리 장치를 이용한 살균 처리법에 주 관심을 두고 있다. 전처리 장치의 효율을 높이는 방법에는 물리적인 방법이나 화학적인 방법, 생물학적인 방법 등 여러 가지 접근법이 존재하지만, 물리적인 방법 중 하나인 전극이 생성한 전기장 분포에 대한 연구는 아직 활발히 이루어지지 않았다. 따라서 본 논문은 전극의 형상 변화가 전기장을 어떻게 변화시키는 지에 대한 경향성 및 최적화 연구를 목표로 두었다. 얻어진 연구 결과로부터 어떤 형상의 전극이 최적의 전기 분해 효율을 가져오는지 알아낼 수 있다.

본 논문은 다음과 같은 내용으로 구성되어있다. 정전기 문제의 지배 방정식으로부터, 유한 요소 해석을 위한 약식(weak form)이 유도되었다. 그리고 그 방정식으로부터 정전기 문제에 대한 연속체 기반 설계 감도 분석 (DSA) 방법이 유도 되었습니다. 이 때, 고차 목적 함수를 고려하기 위한 해석 및 DSA 방법을 위해 9 노드 FEM 기반 함수를 형상 함수로서 사용한다. DSA 방법을 통해 얻어진 민감도 값을 목적 함수에 대한 설계 변수의 경향성으로 생각할 수 있고, 이를 이용해 최적화 연구를 진행한다. 최적화를 진행할 때, 형상 최적화 설계에서 설계 변수를 지정하는 것은 중요한 이슈이다. 설계 변수가 너무 많으면 생산할 수 없는 불규칙한 경계를 가진 최적 형상을 결과로서 제시할 가능성이 있기 때문이다. 이를 방지 하기 위해

설계 변수를 B- 스플라인 함수로 매개 변수화 하였고, 부드러운 경계 변형을 얻어내었다. 또한 최적화 설계의 고질적인 문제로서 매 최적화 시행 마다 구조물의 모양이 변경되어 메쉬 품질이 크게 떨어지는 문제가 있다. 최적화 과정에서 메쉬 얽힘 문제를 해결하기 위해 메쉬 정규화 방법(Mesh regularization scheme)이 사용되었다. 본 방법에서는 디리쉴릿(dirichlet) 에너지 함수를 최소화함으로써 메쉬 균일 성을 자동으로 얻을 수 있다.

연구 결과의 수치 시뮬레이션을 검증하기 위해 수치 예제를 Comsol 소프트웨어 결과와 비교하였다. 해석 결과는 Comsol 소프트웨어 결과와 비교 분석하였고, DSA 방법을 통해 얻어진 민감도 값은 잘 알려진 유한차분법을 통해 검증되었다. 얻어진 민감도 값과 형상 설계 최적화 기법을 이용해 주어진 목적 함수와 제한 조건하에서 최적의 전극 형상을 얻어낸다. 목적함수를 전기 분해 효율과 관련된 값으로 두어 최적 전극 형상의 기하 특성 및 최적화 진행 과정을 구체적으로 논의한다. 마지막으로, 향후 연구를 위해 전극 형태의 파라 메트릭 연구가 3D 환경에서 수행되었다. 3D에서의 형상 설계 최적화를 진행하려면 너무 많은 계산 비용을 필요로 하기 때문에 파라 메트릭 연구를 통해, 전극의 기하 특성과 전기 분해 효율에 대한 경향성 연구만을 진행한다. 파라 메트릭 연구를 통해 얻은 결과를 기반으로 3D 환경에서 전극 형상 최적화의 방향을 제시하는 것으로 본 연구를 마무리하였다.

주요어: 정적 전기장 문제, 형상 설계 민감도, 최적 전극 형상, 메쉬 정규화, 3D 파라메트릭 연구

학 번: 2016-21140

Table of Contents

List of Tables

List of Figures

1. Introduction

The electric field generated by the electrode can be applied in various fields in engineering. One example is the DEP phenomenon, which makes it easy to handle nano-sized particles that have traditionally been difficult to handle with mechanical forces by forming a suitable electric field according to the purpose[1]. This means that the particles move under a non-uniform electric field in a specific direction. Studies dealing with nano-sized particles using dielectrophoresis have been widely carried out as follows: particle separation [2], cell manipulation [3], separation for ballast water [4], separation of Bacteria [5], DNA analysis [6], Graphene sensor for Nitric Oxide Detection [7]. In the shipbuilding marine engineering field, electric field analysis is carried out in the process of disinfecting ship ballast water. IMO regulations have made regulations on the quality of ballast water discharged to the oceans more stringent. Therefore, there has been actively studied an electrolysis method capable of sterilizing the ballast water simply and effectively[8-9]. However, no study has been done to find out which shape electrode has the highest electrolysis efficiency by applying the optimum design technique. By changing electrode shape appropriately, the shape and size of the electric field which can be applied to engineering problems can be obtained.

To further expand these studies it is important to obtain an appropriate electric field for the purpose. In general, the influence of the electric field is also influenced by the material properties of the particles or medium to be treated, the shape of the electrode is also greatly influenced [10--12]. Therefore, this paper aims to study the electrode with the optimal shape to produce the appropriate electric field according to the purpose. In order to

achieve this goal, Yoon [10] used a topology optimization technique to obtain a non-uniform electric field of high intensity. However, topology optimization has disadvantages in that the boundary of the obtained optimal shape is discrete, the distinction of the structure boundary is not clear, and the optimal shape with low productivity is obtained [13]. In addition, the topology optimization has a disadvantage in that it is difficult to precisely apply the non-homogeneous dirichlet boundary condition on the electrode during the optimization process. On the other hand, in optimization of shape design, it is easy to maintain dirichlet boundary condition during the optimization process, and since only the boundary nodes on the electrode are design variables, the optimum shape with high productivity can be obtained. There is also a paper on the optimal shape of electrodes using genetic algorithm optimization techniques, genetic algorithm optimization requires a high performance computation device and long computation time, which limits the methodology[12]. Therefore, this research uses shape design optimization as optimization method.

In this study, we study the gradient - based shape design optimization using Finite Element Method. The easiest design variable choice in the shape design optimization is the nodal coordinate of the finite element model, but in this case it is difficult to obtain an unrealistic model with irregular boundary due to too many design variables and to maintain an adequate finite element mesh in the optimization process [14]. Azegami theoretically discussed with the irregular design of shape optimization problems due to the ill-posedness that occurred when a gradient method in Hilbert space was applied directly [15]. Therefore, in order to solve this problem, we apply the following methods to the optimization process.

First, the design velocity field, defined as the mapping rate between the original and the perturbed domain, is expressed by parameterizing the B-

spline function through some nodal coordinates on the electrode boundary. In shape design optimization using FEM, proper selection of design parameterization is very crucial and B-spline function is known as a curve that causes smooth variations [14]. Parameterization into a B-spline function through a few nodal coordinates which reduces the design space yields a much smoother design velocity field and optimal boundary than a conventional irregular boundary. Continuum-based sensitivity analysis is performed using the obtained parameterized design velocity field.

Second, the mesh regularization scheme was used for every optimization iteration to maintain high mesh quality. In shape design optimization, boundary variation occurs at every optimization iteration. Therefore, the nodal coordinates inside the domain must be updated to prevent mesh distortion problem. Since mesh quality in FEM has a great influence on the accuracy of the analysis, it is necessary to maintain high mesh quality through the appropriate mesh update scheme or re-meshing scheme in the middle of the optimization process. The re-meshing procedure has the disadvantage that the optimization convergence may be deteriorated due to a sudden change of the mesh structure, and the original nodal connectivity is lost. Various mesh update schemes have been studied to minimize the use of re-meshing schemes. The linear elasticity problem where boundary variation is the prescribed displacement is solved[16-17] and based on the harmonic mapping theory, there are methods to optimize the functional corresponding to Laplace's equation [18-19]. This functional, however, does not guarantee that the stationary solution satisfies the Laplace's equation, but gives a significantly deteriorated domain parameterization at the concave boundary. So, in this research we use the mesh regularization scheme of Choi [20]. The method minimizes the Dirichlet energy function to obtain effective mapping

between the parametric domain and the physical domain, and the variance of the Jacobian is minimized to obtain the mesh uniformity.

This paper is organized as follows. In Chapter 2, we describe the governing equations and FEM formulations of an electrostatic problem for modeling an electrode. In Chapter 3, FEM-based shape sensitivity expressions are derived. The shape sensitivity expressions corresponding to the objective function will be derived analytically based on the governing equation. In Chapter 4, we will introduce some techniques that are used to obtain smooth boundaries and lower numerical instability in FEM-based shape optimization. First, we describe the shape-design parameterization in which design variables are parameterized using the B-spline function. Second, we describe how the mesh regularization scheme in this methodology is applied in FEM. In Chapter 5, the methodology presented in this paper is verified. First, the analysis results based on the governing equation derived in Chapter 2 are compared with the numerical results using Comsol software which is widely used analysis software. Second, the sensitivity result based on the sensitivity formulation derived in Chapter 3 is compared with the sensitivity result obtained using the Finite Difference Method. Third, we verify our proposed optimization method through optimal electrode design and optimization history with some 2D examples. Fourth, A parametric study was performed using Comsol software to study the optimal shape of electrodes in 3D. In 3D, much more complicated calculations are required because the shape of the electrode in the thickness direction must be taken into consideration. Therefore, we try to explore the characteristics of the optimal electrode shape in 3D by changing various parameters that determine the shape of the electrode. And finally for conclusion, this paper will end by summarizing some conclusions derived from this research and presenting topics that can be studied in the future.

2. Finite element analysis of electrostatic problem

2.1 Governing equations

Generally, an electric field is formed by being coupled with a magnetic field. However, this problem is a time-independent problem because it assumes that DC is applied to the Electrode instead of AC. Therefore, we consider this problem as an electro-static problem with no electric field generated by the magnetic field. Consider the electrostatic problem shown in <Fig. 1>.

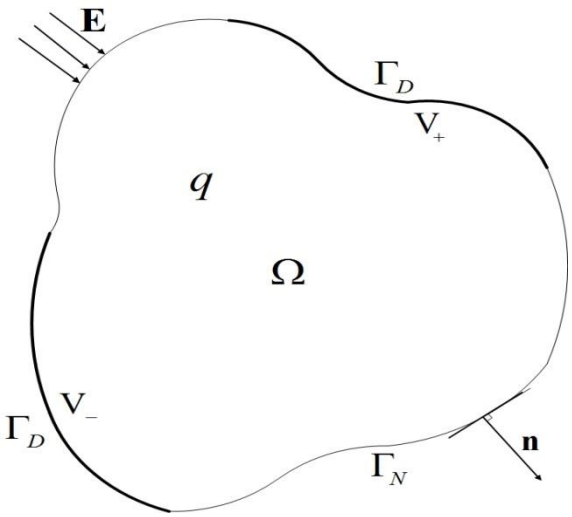

<Fig. 1 Electrostatic problem>

The body occupies an open domain Ω bounded by a closed surface Γ. The boundaries are composed of a prescribed electric potential boundary Γ^D (where Dirichlet boundary condition is imposed) and a prescribed traction boundary Γ^N and mutually disjointed as:

$$\Gamma = \Gamma^D \cup \Gamma^N \text{ and } \Gamma^D \cap \Gamma^N = \phi. \tag{2.1}$$

The body is subjected to the electric charge density q and the prescribed

electric field $\mathbf{E}$ on Γ^N. $\mathbf{n}$ is an outward unit vector normal to the boundary. For a linear and isotropic material constitutive relation, the governing equations of electrostatics are

$$\nabla \cdot \mathbf{E} = \frac{q}{\varepsilon}, \tag{2.2}$$

and

$$\nabla \times \mathbf{E} = 0, \tag{2.3}$$

where ε is permittivity of the media and $\mathbf{E}$ is electric field. Equation (2.2) means that the electric flux passing through the closed surface is equal to the total charge in the closed surface divided by the dielectric constant and (2.3) means the time rate of change of the magnetic flux doesn't exist which is known as Faraday's law. By using introducing following scalar electric potential V, the electric field $\mathbf{E}$ can be expressed as

$$\mathbf{E} = -\nabla \mathrm{V}. \tag{2.4}$$

With above relation, equation (2.3) can be automatically satisfied. By putting equation (2.4) to (2.2), the following equation can be satisfied.

$$-\varepsilon \nabla^2 \mathrm{V} = q. \tag{2.5}$$

In addition to the governing equation (2.5), the dirichlet boundary condition is imposed as

$$\mathrm{V} = \mathrm{V}_0 \ \text{on} \ \Gamma^D. \tag{2.6}$$

For imposing boundary condition (2.6) into the trial solution space directly, the trial solution space Y is defined as

$$\mathrm{Y} = \{\mathrm{V} \in H^1(\Omega) : \mathrm{V} = \mathrm{V}_0 \ \text{on} \ \Gamma^D\}. \tag{2.7}$$

and the space $\bar{\mathrm{Y}}$ for the virtual temperature field as

$$\bar{\mathrm{Y}} = \{\bar{\mathrm{V}} \in H^1(\Omega) : \bar{\mathrm{V}} = 0 \text{ on } \Gamma^D\}. \tag{2.8}$$

Using the virtual electric potential field $\bar{\mathrm{V}}$ that satisfies the homogeneous boundary conditions, the weak form of equation (2.5) is written as

$$\int_\Omega (-\varepsilon \nabla^2 \mathrm{V} - q)\,\bar{\mathrm{V}}\, d\Omega = 0 \quad \text{for all } \bar{\mathrm{V}} \in \bar{\mathrm{Y}}. \tag{2.9}$$

Using the condition in equation (2.8) and divergence theorem, the equation (2.9) can be rewritten as

$$\int_\Omega \varepsilon \nabla \bar{\mathrm{V}} \cdot \nabla \mathrm{V}\, d\Omega = \int_\Omega q\,\bar{\mathrm{V}}\, d\Omega - \int_{\Gamma^N} \varepsilon(\bar{\mathrm{V}}\mathbf{E}\cdot\mathbf{n}) d\Gamma^N \quad \text{for all } \bar{\mathrm{V}} \in \bar{\mathrm{Y}}, \tag{2.10}$$

A bilinear electric energy form is defined as

$$a(\mathrm{V}, \bar{\mathrm{V}}) \equiv \int_\Omega \varepsilon \nabla \mathrm{V} \cdot \nabla \bar{\mathrm{V}}\, d\Omega. \tag{2.11}$$

and a linear load form is defined as

$$\ell(\bar{\mathrm{V}}) \equiv \int_\Omega q\,\bar{\mathrm{V}}\, d\Omega - \int_{\Gamma^N} \varepsilon(\bar{\mathrm{V}}\mathbf{E}\cdot\mathbf{n}) d\Gamma^N. \tag{2.12}$$

2.2 Finite element formulation

Since the objective function can include second derivative of the response, we will use general quadratic shape function for approximating geometry and response[21]. The positions of 9-nodes are shown in <Fig. 2>.

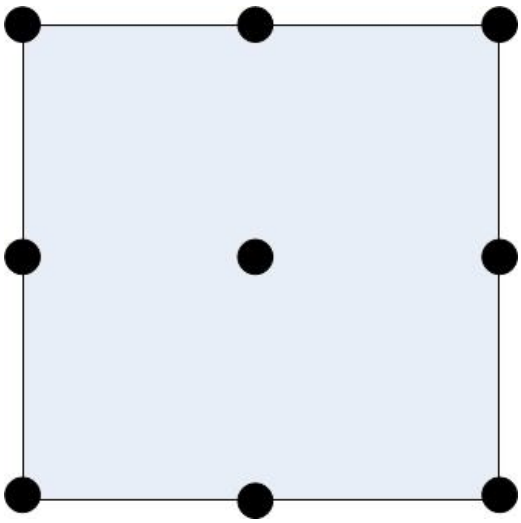

<Fig. 2 9-node element in Finite Element Analysis>

For an element, by using an iso-parametric mapping, geometries and responses are expressed

$$\begin{aligned} x(\xi,\eta) &= \sum_i N_i(\xi,\eta)x_i \\ y(\xi,\eta) &= \sum_i N_i(\xi,\eta)y_i, \end{aligned} \tag{2.13}$$

and

$$\mathrm{V}(\xi,\eta) = \sum_i N_i(\xi,\eta)\,\mathrm{V}_i, \tag{2.14}$$

where x_i, y_i is the nodal coordinate each in the x, y direction and V_i is electric potential on the node. The variational equation (2.10) can be written as

$$a(\mathrm{V},\bar{\mathrm{V}}) = \ell(\bar{\mathrm{V}}), \quad \text{for all } \bar{\mathrm{V}} \in \bar{\mathrm{Y}}. \tag{2.15}$$

3. Shape design optimization

3.1 Material derivative

Consider the variation of domain from an original domain Ω to a perturbed domain Ω_τ as shown in <Fig. 3>.

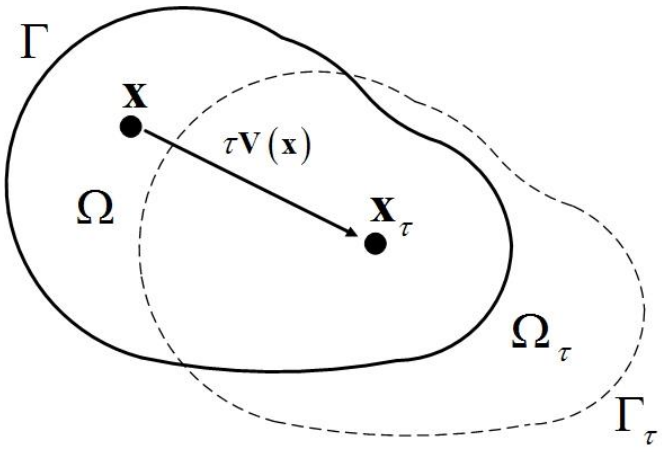

< Fig. 3 Variation of domain>

Suppose that only one parameter τ defines a transformation T. The mapping $T:\mathbf{x}\to\mathbf{x}_\tau$, $\mathbf{x}\in\Omega$ is given by:

$$\mathbf{x}_\tau \equiv T(\mathbf{x},\tau), \tag{3.1}$$

and

$$\Omega_\tau \equiv T(\Omega,\tau). \tag{3.2}$$

A design velocity field $\mathbf{S}$ that is equivalent to a mapping rate can be defined as:

$$\mathbf{S}(\mathbf{x}_\tau,\tau)=\frac{d\mathbf{x}_\tau}{d\tau}=\frac{dT(\mathbf{x},\tau)}{d\tau}=\frac{\partial T(\mathbf{x},\tau)}{\partial\tau}. \tag{3.3}$$

The point-wise material derivative of response V at $\mathbf{x}\in\Omega$ is expressed as:

$$\dot{\mathbf{V}} \equiv \frac{d}{d\tau}\mathbf{V}_\tau(\mathbf{x}+\tau S(\mathbf{x}))\Big|_{\tau=0} = \mathbf{V}' + \nabla\mathbf{V}\cdot\mathbf{S}, \tag{3.4}$$

where $\mathbf{V}'$ and $\nabla\mathbf{V}$ are the partial derivative and gradient of $\mathbf{V}$, respectively. One attractive feature of the partial derivative is that, with an assumption of smoothness, the differentiation order between it and the spatial derivative are interchangeable, because both are independent, that is,

$$(\nabla\mathbf{V})' = \nabla(\mathbf{V}'). \tag{3.5}$$

Consider the objective function in domain and boundary integral forms:

$$\psi_1 = \int_\Omega f(\mathbf{x})\, d\Omega, \tag{3.6}$$

and

$$\psi_2 = \int_\Gamma g(\mathbf{x})\, d\Gamma.$$

The first order variations with respect to the shape design parameter τ are derived as:

$$\begin{aligned}\psi_1' &\equiv \frac{d}{d\tau}\int_{\Omega_\tau} f_\tau(\mathbf{x}_\tau)\, d\Omega_\tau\Big|_{\tau=0} = \int_\Omega \frac{d}{d\tau}\{f_\tau(\mathbf{x}_\tau)|\mathbf{J}|\}\Big|_{\tau=0} d\Omega \\ &= \int_\Omega \{f'(\mathbf{x}) + \nabla f(\mathbf{x})\cdot\mathbf{S}(\mathbf{x}) + f(\mathbf{x})\, div(S(\mathbf{x}))\}\, d\Omega \\ &= \int_\Omega \{f'(\mathbf{x}) + div(f(\mathbf{x})\mathbf{S}(\mathbf{x}))\}\, d\Omega,\end{aligned} \tag{3.7}$$

and

$$\begin{aligned}\psi_2' &\equiv \frac{d}{d\tau}\int_{\Gamma_\tau} g_\tau(\mathbf{x}_\tau)\, d\Gamma_\tau\Big|_{\tau=0} = \int_\Omega \frac{d}{d\tau}\{g_\tau(\mathbf{x}_\tau)|\mathbf{J}|\|\mathbf{J}^{-T}\mathbf{n}\|\}\Big|_{\tau=0} d\Gamma \\ &= \int_\Omega \{g'(\mathbf{x}) + (\nabla g(\mathbf{x})\cdot\mathbf{n} + \kappa g(\mathbf{x}))\mathbf{S}(\mathbf{x})\cdot\mathbf{n}\}\, d\Gamma,\end{aligned} \tag{3.8}$$

where $\kappa = div(\mathbf{n})$ is used. For a detailed derivation of shape sensitivity expressions, the interested readers may refer to Haug et al. [22].

3.2 Shape sensitivity analysis – direct differentiation method

Taking the first order variation of the bilinear electric energy form and linear load form which respect to shape design parameter τ, we have the followings:

$$[a(\mathrm{V},\bar{\mathrm{V}})]' = a'(\mathrm{V},\bar{\mathrm{V}}) + a(\mathrm{V}',\bar{\mathrm{V}}) + a(\mathrm{V},\bar{\mathrm{V}}'), \tag{3.9}$$

and

$$[\ell(\bar{\mathrm{V}})]' = \ell'(\bar{\mathrm{V}}) + \ell(\bar{\mathrm{V}}'), \tag{3.10}$$

where $a'(\mathrm{V},\bar{\mathrm{V}})$ and $\ell'(\bar{\mathrm{V}})$ denote the explicit variation terms with the dependence of their arguments on the shape design parameter suppressed. For brevity of the problem, the external loads are assumed independent of shape variations. Using the linearity of energy and load forms and the fact that $\mathrm{V}' = \dot{\mathrm{V}} - \nabla \mathrm{V}\cdot\mathbf{S}$, equations (3.9) and (3.10) are rewritten as:

$$\begin{aligned}[a(\mathrm{V},\bar{\mathrm{V}})]' &= a'(\mathrm{V},\bar{\mathrm{V}}) + a(\dot{\mathrm{V}} - \nabla \mathrm{V}\cdot\mathbf{S},\bar{\mathrm{V}}) + a(\mathrm{V},\dot{\bar{\mathrm{V}}} - \nabla\bar{\mathrm{V}}\cdot\mathbf{S}) \\ &= a'(\mathrm{V},\bar{\mathrm{V}}) + a(\dot{\mathrm{V}},\bar{\mathrm{V}}) - a(\nabla \mathrm{V}\cdot\mathbf{S},\bar{\mathrm{V}}) \\ &\quad + a(\mathrm{V},\dot{\bar{\mathrm{V}}}) - a(\mathrm{V},\nabla\bar{\mathrm{V}}\cdot\mathbf{S}).\end{aligned} \tag{3.11}$$

and

$$\begin{aligned}[\ell(\bar{\mathrm{V}})]' &= \ell'(\bar{\mathrm{V}}) + \ell(\dot{\bar{\mathrm{V}}} - \nabla\bar{\mathrm{V}}\cdot\mathbf{S}) \\ &= \ell'(\bar{\mathrm{V}}) + \ell(\dot{\bar{\mathrm{V}}}) - \ell(\nabla\bar{\mathrm{V}}\cdot\mathbf{S}).\end{aligned} \tag{3.12}$$

Also, using the fact that $[a(\mathrm{V},\bar{\mathrm{V}})]' = [\ell(\bar{\mathrm{V}})]',\ \forall\bar{\mathrm{V}}\in\bar{\mathrm{Y}},$ and $a(\mathrm{V},\dot{\bar{\mathrm{V}}}) = \ell(\dot{\bar{\mathrm{V}}}),\ \forall\dot{\bar{\mathrm{V}}}\in\bar{\mathrm{Y}},$ the shape sensitivity equations are completely derived as:

$$a(\dot{\mathrm{V}},\bar{\mathrm{V}}) = \ell'_S(\bar{\mathrm{V}}) - a'_S(\mathrm{V},\bar{\mathrm{V}}),\ \forall\bar{\mathrm{V}}\in\bar{\mathrm{Y}}, \tag{3.13}$$

where

$$a(\dot{\mathrm{V}},\bar{\mathrm{V}}) \equiv \int_{\Omega} \nabla\dot{\mathrm{V}}\cdot\nabla\bar{\mathrm{V}}\, d\Omega. \tag{3.14}$$

$$\ell'_S(\bar{\mathrm{V}}) \equiv \ell'(\bar{\mathrm{V}}) - \ell(\nabla\bar{\mathrm{V}}\cdot\mathbf{S}). \tag{3.15}$$

$$a'_S(\mathrm{V},\bar{\mathrm{V}}) = a'(\mathrm{V},\bar{\mathrm{V}}) - a(\nabla\mathrm{V}\cdot\mathbf{S},\bar{\mathrm{V}}) - a(\mathrm{V},\nabla\bar{\mathrm{V}}\cdot\mathbf{S}). \tag{3.16}$$

The load terms are assumed to be independent of shape variations. By solving equation (3.13), response sensitivity $\dot{\mathrm{V}}$ can be obtained. But generally, not all response sensitivities are required to obtain sensitivity of objective function. So, direct differentiation method is somewhat inefficient in terms of computation cost. To improve such a problem, following adjoint variable method can be used to calculate sensitivity of a specific function efficiently.

3.3 Shape sensitivity analysis – adjoint variable method

Consider a general objective function that may be written in integral form as:

$$\psi = \int_{\Omega} \mathrm{g}(\mathrm{V},\nabla\mathrm{V},\nabla(\nabla\mathrm{V}))d\Omega, \tag{3.17}$$

where $\mathrm{V}\in H^2(\Omega)$ and function g is continuously differentiable with respect to its arguments. Note that ψ depends on Ω in two ways. First, there is an obvious dependence of ψ on its integral domain. Second, response variable V depends on domain Ω. By using the material derivative formulas from equation (3.7), the variation of the functional in equation (3.17) can be obtained as:

$$\psi' = \int_{\Omega} \{\mathrm{g}_{,\mathrm{V}}\,\mathrm{V}' + \mathrm{g}_{,\nabla\mathrm{V}}\cdot\nabla\mathrm{V}' + \mathrm{g}_{,\nabla(\nabla\mathrm{V})}\cdot\cdot\nabla(\nabla\mathrm{V}') + div(\mathrm{g}\mathbf{S})\}d\Omega. \tag{3.18}$$

Using the relation in equation (3.4), the partial derivatives in equation (3.18) can be rewritten in terms of $\dot{\mathrm{V}}$ as:

$$\psi' = \int_\Omega \{ g_{,V}\, \dot{V} + g_{,\nabla V} \cdot \nabla \dot{V} + g_{,\nabla(\nabla V)} \cdot\cdot \nabla(\nabla \dot{V}) - g_{,V}\, \nabla V \cdot \mathbf{S} \\ - g_{,\nabla V} \cdot \nabla(\nabla V \cdot \mathbf{S}) - g_{,\nabla(\nabla V)} \cdot\cdot \nabla(\nabla(\nabla V \cdot \mathbf{S})) + div(g\mathbf{S}) \} d\Omega. \tag{3.19}$$

Note that $\dot{V}, \nabla\dot{V},$ and $\nabla(\nabla\dot{V})$ depend on velocity field $\mathbf{S}$. The objective is to obtain an explicit expression for ψ' in terms of $\mathbf{S}$, which requires rewriting the first three terms of the first integral on the right side of equation (3.19) explicitly in terms of $\mathbf{S}$, that is, by eliminating $\dot{V}$.

An adjoint equation is introduced by replacing $\dot{V} \in \bar{Y}$ in equation (3.19) by the virtual electric voltage $\lambda \in \bar{Y}$ and by equating the sum of terms involving $\bar{\lambda}$ with the energy bilinear form, yielding the adjoint equation for the adjoint variable λ as

$$a(\lambda, \bar{\lambda}) = \int_\Omega \{ g_{,V}\, \bar{\lambda} + g_{,\nabla V} \cdot \nabla \bar{\lambda} + g_{,\nabla(\nabla V)} \cdot\cdot \nabla(\nabla \bar{\lambda}) \} d\Omega, \quad \forall \bar{\lambda} \in \bar{Y}. \tag{3.20}$$

To take advantage of the adjoint equation, evaluate equation (3.20) at $\bar{\lambda} = \dot{V} \in \bar{Y}$ to obtain the following expression:

$$a(\lambda, \dot{V}) = \int_\Omega \{ g_{,V}\, \dot{V} + g_{,\nabla V} \cdot \nabla \dot{V} + g_{,\nabla(\nabla V)} \cdot\cdot \nabla(\nabla \dot{V}) \} d\Omega. \tag{3.21}$$

Similarly, the design sensitivity equation (3.13) may be evaluated at $\bar{V} \in \lambda$, since both belong to Y, to obtain

$$a(\dot{V}, \lambda) = \ell'_S(\lambda) - a'_S(V, \lambda). \tag{3.22}$$

Recalling that energy bilinear form $a(\square,\square)$ is symmetric in its arguments, we can conclude that the left sides of equations (3.21) and (3.22) are equal; thus, the right sides of both equations yield the following useful relation:

$$\int_\Omega \{ g_{,V}\, \dot{V} + g_{,\nabla V} \cdot \nabla \dot{V} + g_{,\nabla(\nabla V)} \cdot\cdot \nabla(\nabla \dot{V}) \} d\Omega = \ell'_S(\lambda) - a'_S(V, \lambda). \tag{3.23}$$

By substituting equation (3.23) into equation (3.19), the expression of ψ' in terms of $\mathrm{V}, \lambda,$ and $\mathbf{S}$ is obtained as

$$\begin{aligned}\psi' &= \ell'_S(\lambda) - a'_S(\mathrm{V},\lambda) \\ &\quad - \int_\Omega \{g_{,\mathrm{V}} \nabla \mathrm{V}\cdot\mathbf{S} + g_{,\nabla\mathrm{V}}\cdot\nabla(\nabla \mathrm{V}\cdot\mathbf{S}) + g_{,\nabla(\nabla\mathrm{V})}\cdot\cdot\nabla(\nabla(\nabla \mathrm{V}\cdot\mathbf{S})) + \mathrm{div}(g\mathbf{S})\}\mathrm{d}\Omega \\ &= \ell'(\lambda) - \ell(\nabla\lambda\cdot\mathbf{S}) - a'(\mathrm{V},\lambda) + a(\nabla \mathrm{V}\cdot\mathbf{S},\lambda) + a(\mathrm{V},\nabla\lambda\cdot\mathbf{S}) \\ &\quad - \int_\Omega \{g_{,\mathrm{V}} \nabla \mathrm{V}\cdot\mathbf{S} + g_{,\nabla\mathrm{V}}\cdot\nabla(\nabla \mathrm{V}\cdot\mathbf{S}) + g_{,\nabla(\nabla\mathrm{V})}\cdot\cdot\nabla(\nabla(\nabla \mathrm{V}\cdot\mathbf{S})) + \mathrm{div}(g\mathbf{S})\}\mathrm{d}\Omega\end{aligned} \quad (3.24)$$

Note that the evaluation of the design sensitivity formula in equation (3.24) requires solving the variational equation (2.15) for V. Similarly, the variational adjoint equation (3.20) must be solved for adjoint variable λ. Using finite element analysis, solving for λ is efficient if the boundary−value problem for V has already been solved. This is because the stiffness matrix used in the analysis is the same as the stiffness matrix used to obtain the solution space. It is easy to get λ by calling the same stiffness matrix and replacing the load term with the adjoint load term.

4. Shape design optimization techniques in finite element analysis

4.1 Design variable parameterization

In Finite Element Analysis, the nodal coordinates on boundary are usually taken as shape variables. But this independent nodal movement approach makes very large set of design variables since all nodes on the design boundary must be adopted as design variables. This means that the design variable number on the fine mesh increases exponentially. So usually, the conventional method which takes all boundary nodal points as design variables requires large computation time of the optimization process. Also the conventional method has a tendency to generate unrealistic wiggly designs as shown in <Fig. 4> due to large design space. This unrealistic design not only lowers the manufacturability of the resulting optimal shape, but also does not meet geometrical requirements on the regularity of the boundaries.

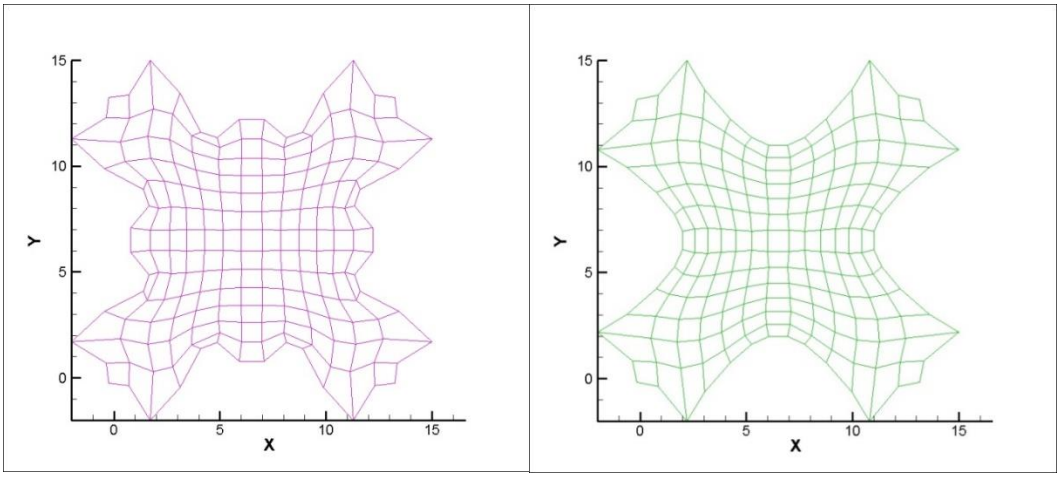

<Fig. 4 Optimal shape obtained by parameterization with optimal shape (left) and obtained without parameterization of design variables (right)>

To solve such problems in taking nodal coordinates on the boundary as

shape variables, the parameterization technique can be used. The parameterization technique is not to take all nodal coordinates on boundaries as design variables, but to take only some representative nodal coordinates as design variables. The key points of this methodology are as follows. 1) Since the sensitivity between adjacent nodal points is approximate, the boundary can be thought of as dividing it into several piece boundaries. 2) Select arbitrarily several representative nodal points on each piece boundary. 3) Optimize by taking only representative nodal points as a design variable. 4) For each iteration step of optimization, each representative nodal points are considered as interpolation points. These points can be connected using appropriate parametric functions to obtain the overall boundary shape. 5) Repeat the method of 4) and optimize until convergence condition is satisfied. With this parameterization method, the number of design variables can be effectively reduced without losing the overall sensitivity tendency. This method leads to a reduction in computation time and a smoother boundaries.

Although various functions can be used as parametric functions, this paper adopts the B-spline function as a parametric function [14]. The B-spline function is easy to express complex geometry with a small set of design variables and is flexible enough to satisfy the regularity constraint at the boundary. Additional control points can be introduced without increasing the degree of the curve. Therefore, parameterization of design variables using B-spline function avoids obtaining unrealistic design. Also, the H-refinement property of the b-spline curve makes it possible to easily calculate interpolation values between design variables.

For an example you can see figure in <Fig. 5>. As shown in the figure, the B-spline curve can be expressed with 4 design variables(blue arrows). And by using the H-refinement characteristic of B-spline function, the values of the

red arrows which are distributed among the design variables can be calculated. H-refinement is a way to increase the number of control points without changing the shape of the b-spline curve. In this methodology, the control point of b-spline corresponds to a design variable representing the shape of the boundary. Therefore, we can use this property of the b-spline curve to calculate the interpolation value at the desired point without changing the optimal shape resulting from the optimization.

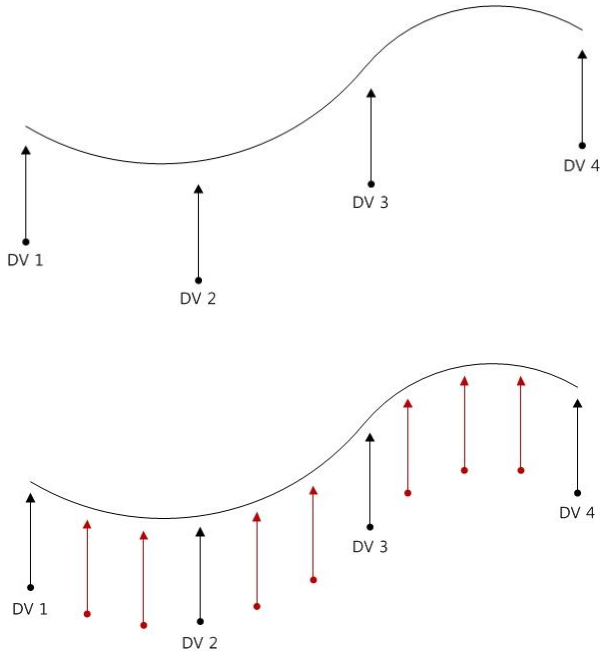

<Fig. 5 Design variables parameterization by using B-spline function>

4.2 Mesh regularization scheme

In finite element analysis, the fact that mesh quality has a significant role in the accuracy of analysis has been widely known. Especially in shape design optimization, since the structure boundary varies at every iteration, maintaining high mesh quality is an important issue. So, it is still an inherent challenge to update inner node coordinates after boundary variation, in order to avoid mesh distortion and maintain high quality of mesh for reliable

response and design sensitivity analysis.

In the shape design optimization based on conventional finite element analysis, re-meshing scheme is generally used to obtain high mesh quality if the boundary variation is significantly large and complicated. However, re-meshing scheme should not be frequently used, since the large variation of mesh structure may lead to sudden variation of the objective function or violation of the constraints which prevents smooth convergence to an optimal shape. Furthermore, when the re-meshing scheme is used, the connectivity between elements and nodes changes due to the change in the mesh structure, resulting in inconvenience in subsequent computations.

Therefore, when performing shape optimization, various methods of maintaining high mesh quality without re-meshing scheme have been studied [16-20]. In this paper, we use a mesh regularization scheme that minimizes the following Dirichlet energy function with convexity properties [20].

$$F_D = \frac{1}{2}\int_X (\|\nabla u_1\|^2 + \|\nabla u_2\|^2) dX = \frac{1}{2}\int_X (u_{1,x_1}{}^2 + u_{1,x_2}{}^2 + u_{2,x_1}{}^2 + u_{2,x_2}{}^2) dX. \quad (4.1)$$

Since the equation (4.1) is convex, the minimization of equation (4.1) is equivalent to satisfying Laplace's equation. If it satisfies Laplace's equations, mapping $\mathbf{F}: X(x_1, x_2) \rightarrow \tilde{X}(u_1, u_2)$ can be achieved and also bijective mapping can be obtained by the RKC theorem [23]. Since the convergence of the Dirichlet energy function is good due to the minimization convergence, a bijective mapping between the parametric and the physical domain can be obtained effectively. In addition, the variance of the Jacobian is minimized and the mesh uniformity is achieved as shown in <Fig. 6>.

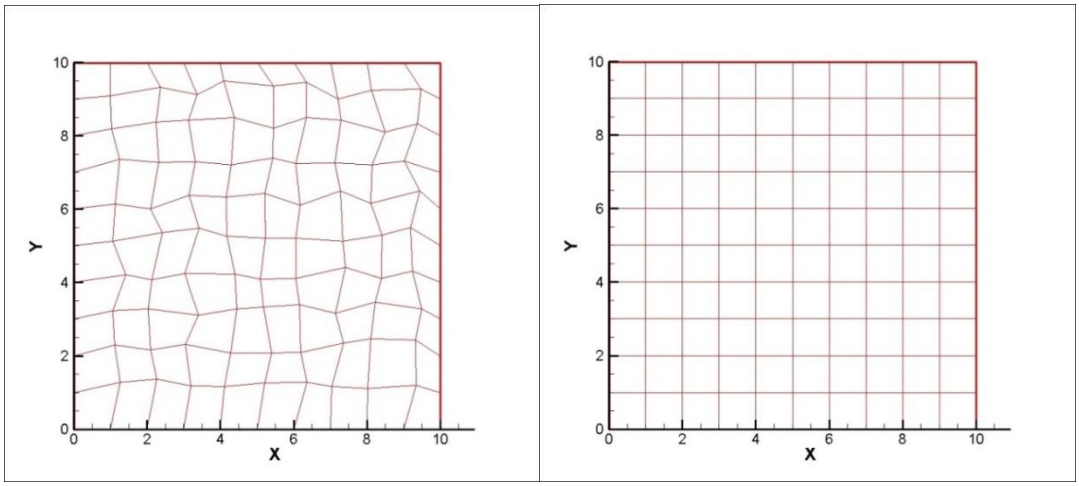

<Fig. 6 Mesh regularization example 1 by minimizing Dirichlet energy functional>

The left figure in <Fig. 6> is the initial entangled mesh, the right figure is the regularized mesh by minimizing Dirichlet energy functional. Initially, the size of each mesh was unevenly distributed and the standard deviation of jacobian was large. However, if the mesh regularization scheme is used, the distribution of the elements can be uniformly obtained as shown in the right figure (mesh uniformity is achieved). Mesh uniformity does not just mean that all elements have the same size. Since this mesh regularization scheme minimizes the standard deviation of the jacobian of all the elements, each element has a proper shape and size according to the characteristics of the geometry where the element is located. For comprehensive understanding, you can see the following figures:

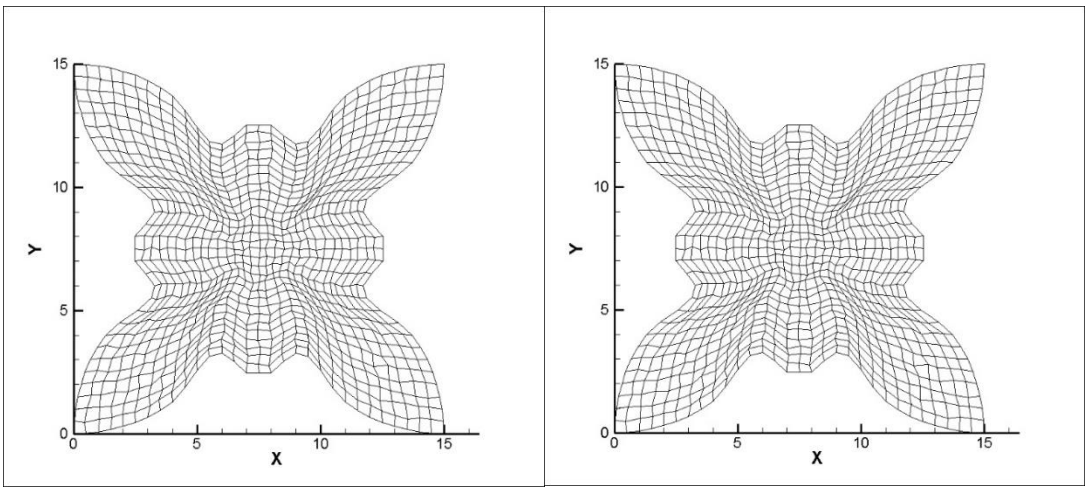

Initial mesh Transient mesh 1

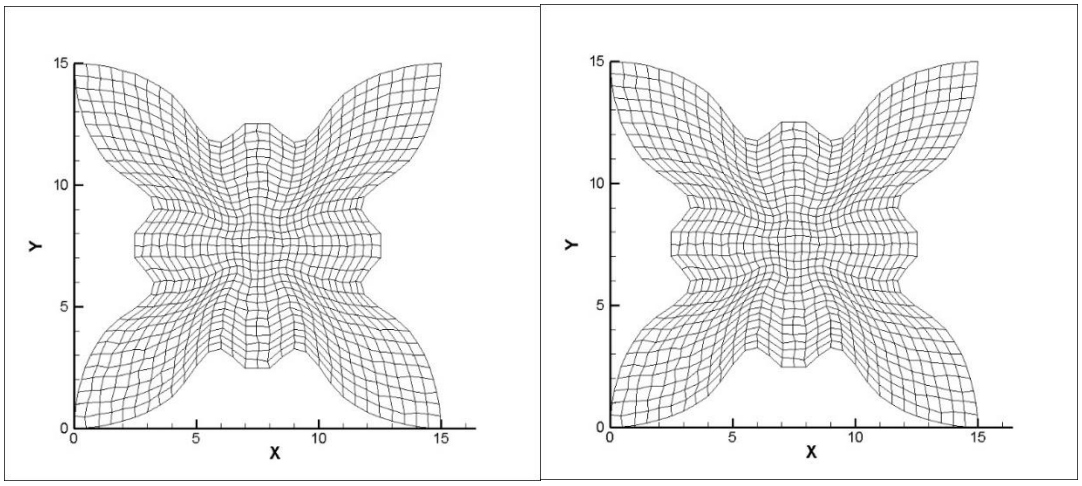

Transient mesh 2 Final mesh

<Fig. 7 Mesh regularization example 2 by minimizing Dirichlet energy functional >

Observing the above figure, it can be seen that the mesh quality becomes higher as the uniformity of each mesh is gradually satisfied in the first meshing state during the mesh regularization scheme. Of course, using this methodology has the disadvantage that more computation is required for every optimization iteration, but it guarantees better convergence and accuracy in every iteration that mesh quality is updated according to the optimization result.

5. Numerical examples

In this chapter, we demonstrate the effectiveness of the methodologies presented in this paper using various numerical examples. Section 5.1 uses the equations in Chapter 2 to verify the accuracy of the analysis results obtained. The accuracy is verified by comparison with the analysis result obtained using Comsol software for the same model. Next, the sensitivity formulation derived from Chapter 3 in Section 5.2 is verified using the Finite difference method. In Section 5.3, shape design optimization is performed on 2D electrodes using the shape sensitivities derived from Chapter 3 and the techniques described in Chapter 4. Finally, Section 5.4 presents a directional study of electrode shape optimization in 3D through a parametric study to observe the changes in total electric energy according to the shape and arrangement of 3D electrodes.

5.1 Comparison of analysis results with Comsol software

Our source code was used to analyze the electro-static problem to obtain numerical results. Verification of the numerical results obtained is required. In this research, Comsol software was used to verify the numerical example. Since Comsol software is a commonly used analysis software, its accuracy has already been verified.

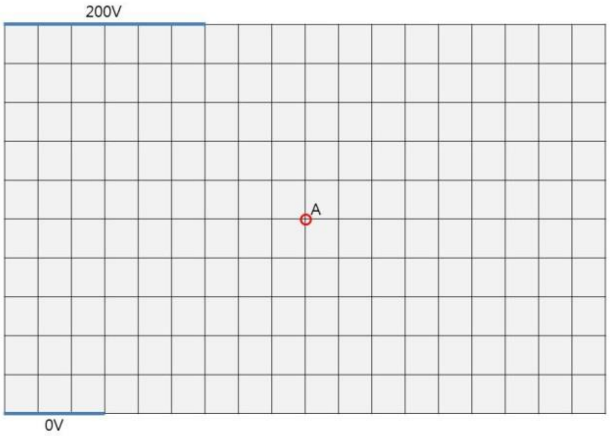

<Fig. 8 Problem example 1>

As described above figure, the square discretization was performed on the rectangular model 18 m long and 10 m long by the square. The upper nodes on blue boundary are imposed 200V electric potential and the lower nodes on blue boundary are imposed 0V electric potential. Compared with Comsol software, the response(potential) contour for the above model are as follows:

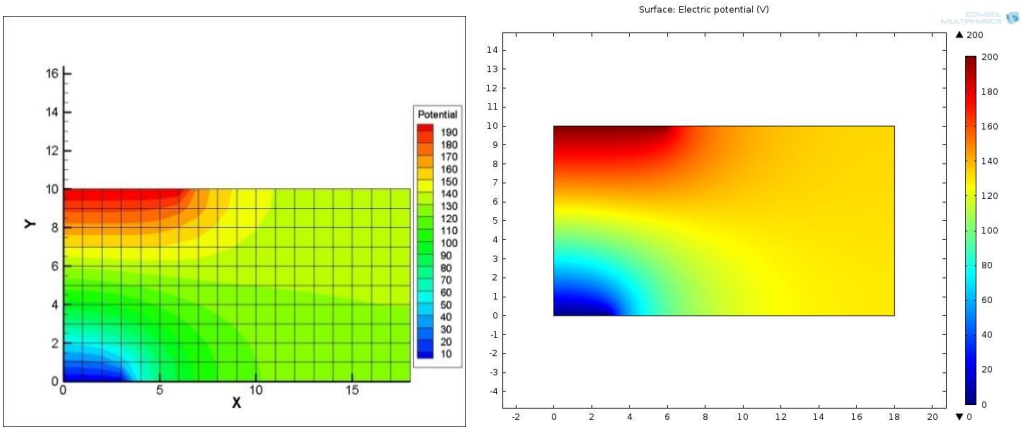

<Fig. 9 Numerical analysis result(left) & Comsol analysis result(right)>

As shown in the above figure, we can see that the contour of the potential corresponding to the response is the same. In fact, the potential value at Point A shown in <Fig. 8> is compared as follows:

	Code (a)	Comsol (b)	Agreement (a)/(b)
Potential	130.060670503981	130.05913538682606	100.0012 (%)

<Table 1 Potential value comparison at Point A in figure 8 >

As can be seen in the above <Table 1>, we can confirm that the agreement at Point A is high. To see another example, we compared the results of the Comsol analysis with the following example.

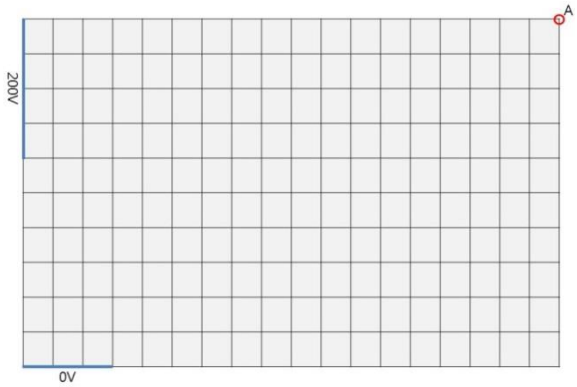

<Fig. 10 Problem example 2>

Similarly, the contour plot of the analysis response for the above model is as follows.

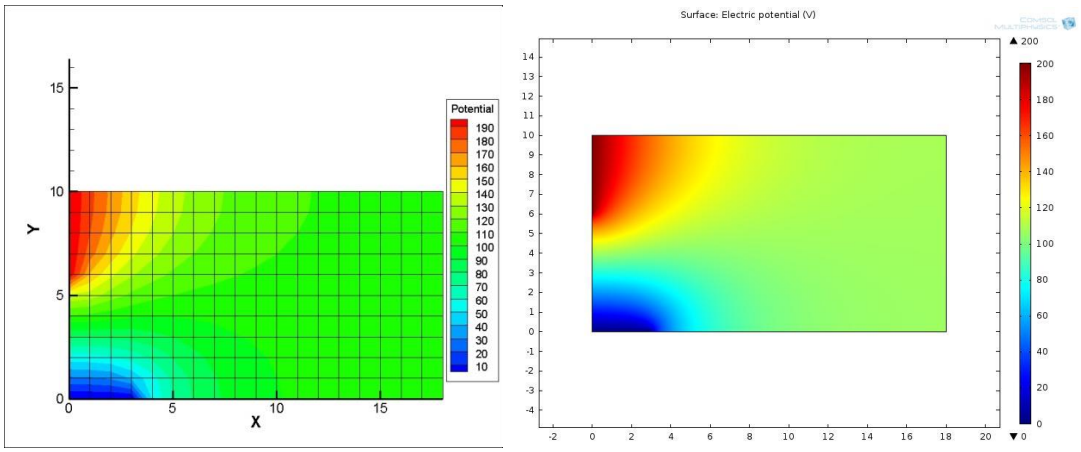

<Fig. 11 Numerical analysis result(left) and Comsol analysis results (right)>

As can be seen in the above figure, we can see that the contour of the

potential corresponding to the response is the same. The potential value at Point A shown in <Fig. 10> is compared as follows:

	Code (a)	Comsol (b)	Agreement (a)/(b)
Potential	107.94124888562	107.946196423368	99.99542 (%)

<Table 2 Potential value comparison at Point A in figure 10 >

In <Table 2>, it can be seen that the agreement at Point A is high. Therefore, it is confirmed that the analysis result using the source code is highly accurate.

5.2. Shape design sensitivity verification

In this section, the derived shape sensitivity is compared with the finite difference sensitivity to verify the derived analytical expressions. The shape sensitivity provides the search direction in gradient based optimization. So accurate shape sensitivity plays a very important role in the shape design optimization, which leads to a correct solution, smooth convergence and reduces time to get an optimal solution. Electrodes for ballast sterilization are often crossed with thin parallel plates[9]. Therefore, in this paper, we try to model and interpret the most basic 2D parallel plate structure as the following figure. Consider a electrostatic problem of a parallel electrode model shown in <Fig. 12>.

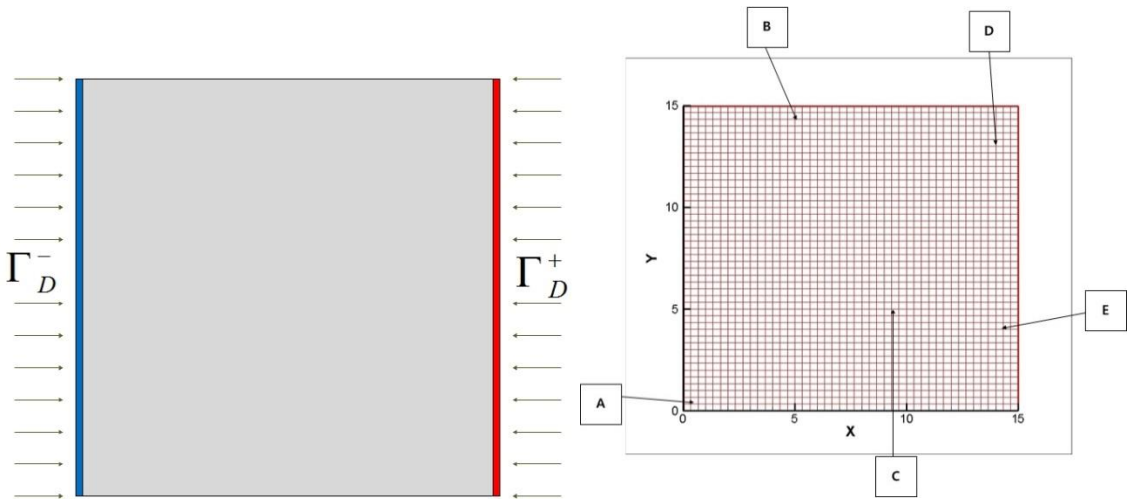

<Fig. 12 Parallel electrode geometry: (a) Problem definition, (b) FEM model>

Γ_D^+ and Γ_D^- are each considered anode and cathode. In anode boundary Γ_D^+ the prescribed electric potential value is 10, and in cathode boundary Γ_D^- the prescribed electric potential value is 0. The parallel electrode geometry model is discretized with 2025 elements and 8281 nodes. To obtain the necessary design velocity field for the shape DSA, the shape variation in <Fig. 12-(a)> is considered. The black arrows represent velocity field which is comprised of all vertical directions to the surface on Dirichlet boundary. As using the design variable parameterization method, we don't need to take all nodes on Dirichlet boundary as design variables to express the design velocity field. We take only 32 nodes to represent design velocity field. The design velocity field is easily obtained from the perturbed node positions.

$$\mathbf{S}(\mathbf{x}) = \sum N_I \delta \mathbf{x}_I . \tag{4.2}$$

where $\delta \mathbf{x}_I$ is the difference of node positions between the original and the perturbed models. So, the design velocity field is also interpolated by the same general 9-node quadratic shape function which is used geometry field expression. The amount of design perturbation is 0.01% and a linear velocity

field is assumed. In <Table 3>, the shape sensitivity of electric voltage from equation (3.24) is compared with the finite difference results. The objective function is the electric voltage on some selected points shown in <Fig. 12-(b)>. As shown in <Table 3>, a good agreement of shape sensitivity is observed.

Position	$V_\tau - V(A)$	$\dot{V}(B)$	$(B)/(A)\times 100(\%)$
A	−2.798506D−001	−2.798506D−001	100.00
B	−1.720692D−002	−1.720692D−002	100.00
C	4.593614D−003	4.593614D−003	100.00
D	2.801250D−002	2.801250D−002	100.00
E	5.998747D−003	5.998747D−003	100.00

<Table 3 Comparison of design sensitivity with finite difference method>

Now that we have obtained very accurate and efficient sensitivity as shown <Table 3>, we are ready to perform shape design optimization for the electrostatic problem.

5.3. Shape design optimization for 2D electrodes

Some numerical examples for the shape optimization are demonstrated to show the applicability and effectiveness of the proposed method. In all examples, the permittivity of medium ε is assumed a unit value. Because if the only one kind of medium exists, ε can be considered a constant value which can be eliminated in governing equation (2.5). And also, all kind of load terms in equation (2.12) are assumed to be zero. We only consider electrode shape optimization where electric charge density q and electric flux $\mathbf{E}\cdot\mathbf{n}$ on surface don't exist. Consider an electrostatic problem in which there is only an anode with a value of 10V and a cathode with a value of 0V.

5.3.1. Square-shaped electrode (Total Electric Energy)

In general, the optimization problem has an objective function to maximize (minimizing) and given constraints. For this problem, the objective is to find an optimal design for a maximum Total electric energy which means integration of electric field strengths at a given volumetric. So, we make following objective function for our purpose.

$$\psi = \frac{1}{2}\int_{\Omega_c} (\nabla \mathrm{V}) \cdot (\nabla \mathrm{V}) d\Omega_c. \tag{4.3}$$

where Ω_c is an element located in the center of the whole domain. The shape optimization problem for a maximum total electric energy is stated as

$$\text{Maximize} \quad \frac{1}{2}\int_{\Omega_c} (\nabla \mathrm{V}) \cdot (\nabla \mathrm{V}) d\Omega_c, \tag{4.4}$$

$$\text{Subject to} \quad \int_{\Omega} d\Omega \geq \int_{\Omega_{\text{constraint}}} d\Omega, \tag{4.5}$$

and

$$d_i^{lower} \leq d_i \leq d_i^{upper}, \tag{4.6}$$

where d_i is a design variable set as a nodal point which corresponds to a design boundary along the outer boundary. The shape sensitivity of the volume can be written as

$$\frac{d}{d\tau}\int_{\Omega_\tau} d\Omega_\tau \bigg|_{\tau=0} = \int_{\Omega} \nabla \cdot \mathbf{S} d\Omega. \tag{4.7}$$

For an example, consider a parallelogram 4-electrode square model which is more complicate than basic parallel plate as shown <Fig. 13>. Originally, electrolysis efficiency of parallel plate electrodes should be studied. However,

it is difficult to realize a complicated parallel plate structure due to limitation of modeling in 2D. Therefore, in this paper, we study the tendency of field intensity change according to the electrode shape change by modeling and analyzing a more complicated structure electrode than 2D parallel plate. A study on the electrolytic efficiency of parallel plate electrodes will be done in depth on 3D using COMSOL software.

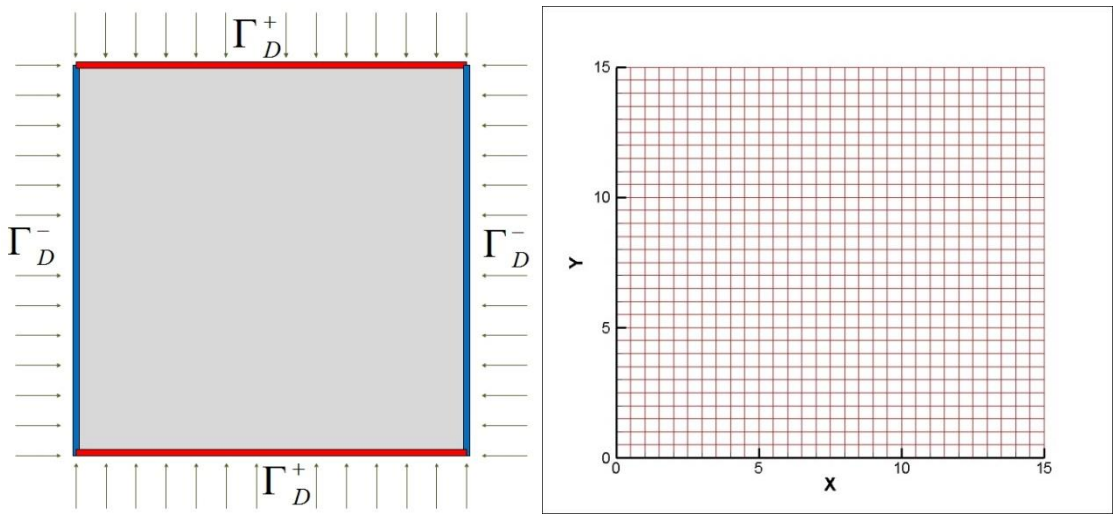

<Fig. 13 4-electrode 4-side geometry: (a) Problem definition, (b) FEM model>

The black arrows represent design velocity field and only 22 nodes on Dirichlet boundary are taken as design variables for design parameterization method. The initial model is discretized with 3721 elements and 900 nodes. The B-spline function order for design variable parameterization is 4 and the constraint volume is 70%. <Fig. 14> shows optimal shape and other results with initial model.

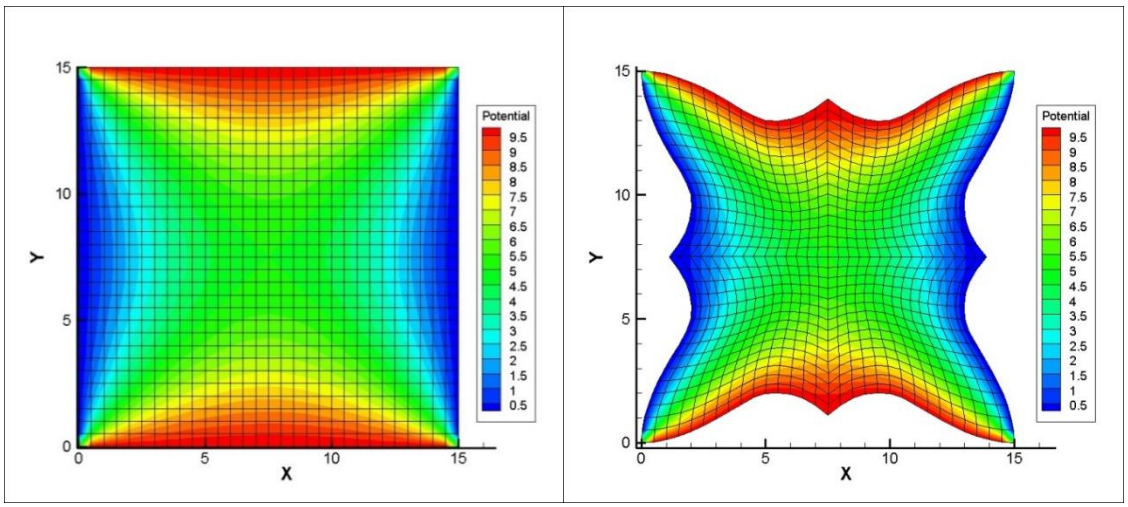

<Fig. 14 Shape optimization result: (a) initial model, (b) optimal model>

The optimal shape, electric potential, and the corresponding nodal points in <Fig. 14-(a)> are compared with those of the initial design <Fig. 14(b)>. The objective function of this problem is set to maximize the electric field energy of the central part. As a result of the optimization, it can be seen that a W-shaped electrode bent toward the center is obtained. This will result in a complex change in the midfield electric field gradient value and an increase in energy over the whole range.

If we apply the tendency of this result to the 2d parallel plate electrolytic device, it can be expected that the better electrolytic effect can be obtained by giving more flexion to the parallel plate. Or the intersection of the parallel plates may be bent to induce the complexity of the electric field gradient value. The nodal points are updated by the MMFD optimization algorithm, based on the analytical shape sensitivities. As shown in the above figure, it can be seen that the central boundary is optimized with sharp curvature because maximizing the electric energy intensity of the center part is an objective function.

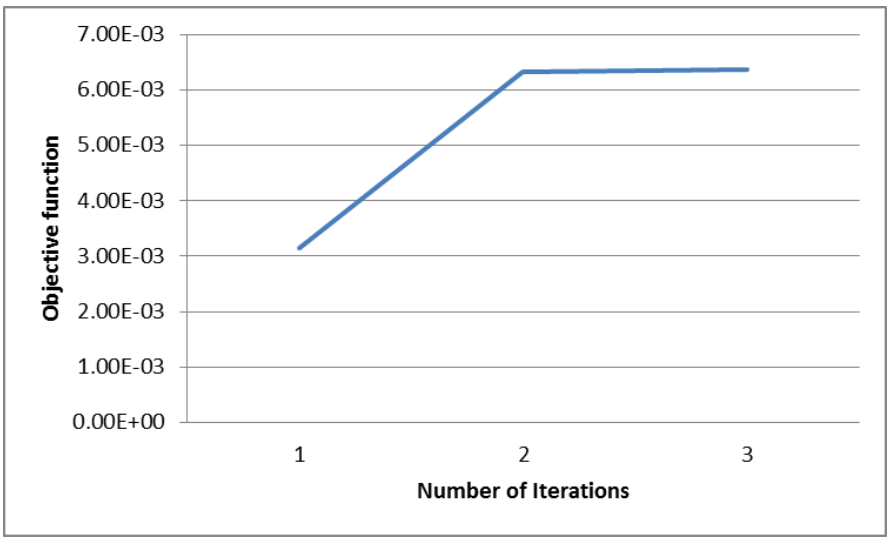

<Fig. 15 Shape optimization history>

<Fig. 15> shows the optimization histories of the objective function. The iteration number is counted only when gradient calculation is called. The objective function increased gradually for 3 iterations, which turns out the proposed method of shape optimization is effective.

5.3.2. Square-shaped electrode with complicated design boundary (Total Electric Energy)

A more complicated 8-electrode model discretized with 3721 nodes and 900 elements is shown in <Fig. 16>. The objective function and constraint volume are the same with previous example. The B-spline function order for design variable parameterization is 2 and the constraint volume is 60%.

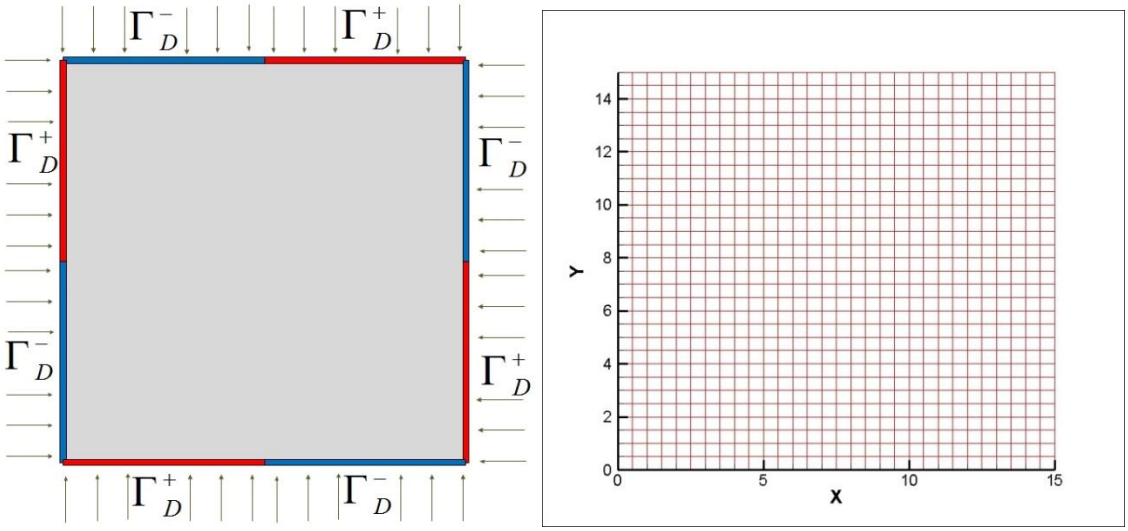

<Fig. 16 8−electrode 4−side geometry: (a) Problem definition, (b) FEM model>

With the initial model and design velocity field in <Fig. 16>, the optimal shape and other results are shown in <Fig. 17>.

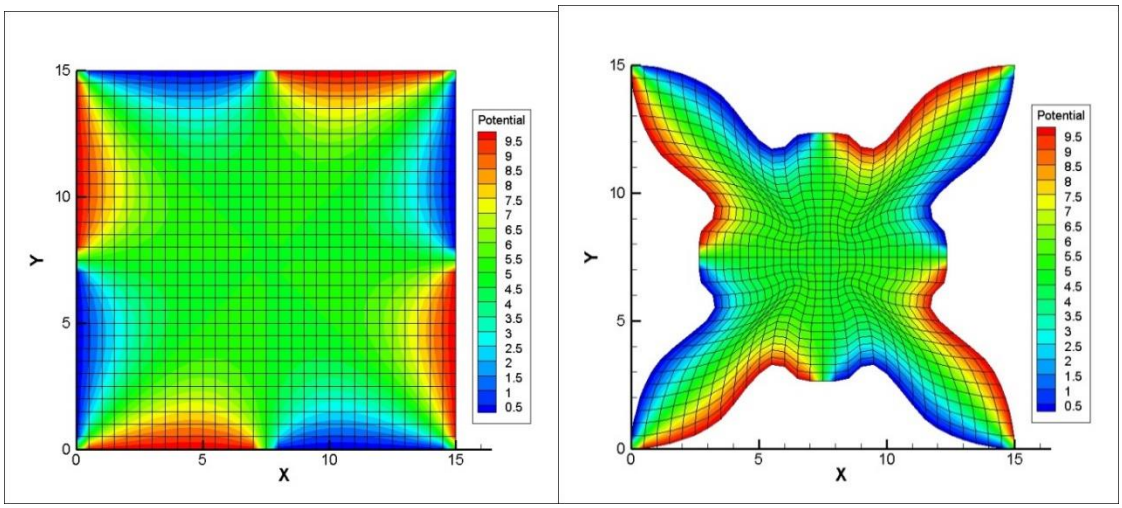

<Fig. 17 Shape optimization result: (a) initial model, (b) optimal model>

It can be seen that the W−shaped curvature is formed toward the central portion as in the previous optimization result. The boundary conditions are a bit more complicated, so they are bent a little more sharply in the middle due to the high freedom. The similar optimal shape was obtained even though the

boundary condition of the electrode was modified, which is a valid simulation result. And also, this result is natural because it uses the same objective function as the previous example. Therefore, we can see that the shape of the electrode which dents the central part in the shape of W maximizes the strength of the electric field center.

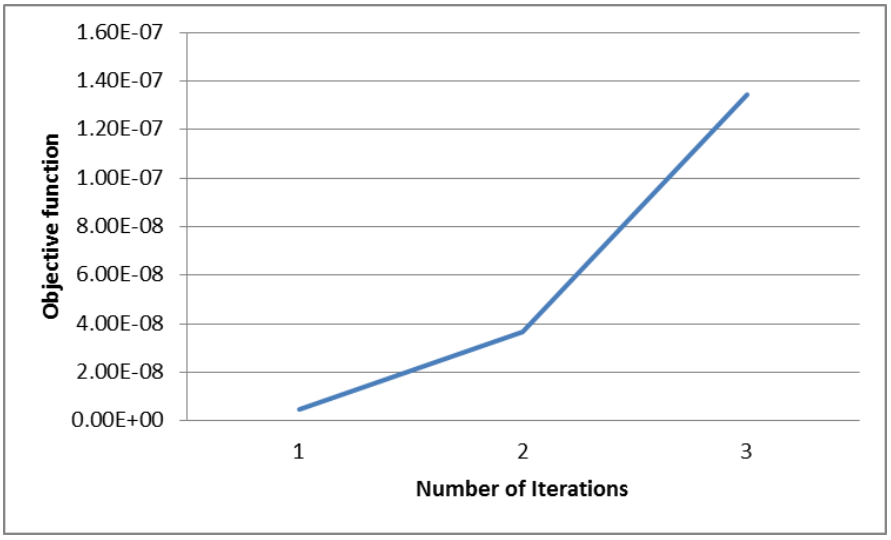

<Fig. 18 Shape optimization history>

<Fig. 18> shows the optimization histories of the objective function. It also shows smooth convergence history.

5.3.3. Square-shaped electrode (DEP Force)

In this example, we want to show the result of optimization by placing another objective function. The objective is to find an optimal design for a maximum DEP force. DEP force is one of the useful techniques for dealing with the movement of fine nanoparticles. In fact, studies have been made on electrodes using DEP force to separate microalgae cells from ballast water of ship[4]. DEP force can be calculated as follows:

$$\mathbf{F}_{DEP} = 2\pi\varepsilon_m r^3 \,\mathrm{Re}(f_{\mathrm{CM}})\nabla|\mathbf{E}|^2, \qquad (4.8)$$

where ε_m is the absolute dielectric permittivity of medium, r is the radius of a particle, f_{CM}, the Clausisus-Mossoti factor, is defined as follows

$$f_{\mathrm{CM}} = \frac{\varepsilon_{\mathrm{p}}^* - \varepsilon_{\mathrm{p}}^*}{\varepsilon_{\mathrm{p}}^* + 2\varepsilon_{\mathrm{m}}^*} \left(\varepsilon_{\mathrm{p}}^* = \varepsilon_{\mathrm{p}} - j\frac{\sigma_{\mathrm{p}}}{\omega}, \varepsilon_{\mathrm{m}}^* = \varepsilon_{\mathrm{m}} - j\frac{\sigma_{\mathrm{m}}}{\omega} \right), \tag{4.9}$$

where the complex permittivity of the particle and its suspending medium are $\varepsilon_{\mathrm{p}}^*$ and $\varepsilon_{\mathrm{m}}^*$, respectively. These kinds of parameters are related with the characteristics of a particle and medium which are not controllable by experiment. So, to maximize DEF force, it is realistic to find we can maximize the square of the electric field gradient $\nabla|\mathbf{E}|^2$. Considering the relation of $\mathbf{E} = -\nabla \mathrm{V}$, we can express $\nabla|\mathbf{E}|^2$ as follows:

$$\nabla|\mathbf{E}|^2 = \nabla(\mathbf{E}\cdot\mathbf{E}) = 2(\nabla\mathbf{E})\cdot\mathbf{E} = 2(\nabla(\nabla \mathrm{V}))\cdot\nabla \mathrm{V}. \tag{4.10}$$

So, we make following objective function for our purpose.

$$\psi = \frac{1}{2}\int_{\Omega_c} \{(\nabla(\nabla \mathrm{V}))\cdot\nabla \mathrm{V}\}\cdot\{(\nabla(\nabla \mathrm{V}))\cdot\nabla \mathrm{V}\} d\Omega_c, \tag{4.11}$$

where Ω_c is an element located in the center of the whole domain where the electric field is distributed. The shape optimization problem for a maximum DEP force at the center point is stated as

$$\text{Maximize} \quad \psi = \frac{1}{2}\int_{\Omega_c} \{(\nabla(\nabla \mathrm{V}))\cdot\nabla \mathrm{V}\}\cdot\{(\nabla(\nabla \mathrm{V}))\cdot\nabla \mathrm{V}\} d\Omega_c, \tag{4.12}$$

$$\text{Subject to} \quad \int_{\Omega} d\Omega \geq \int_{\Omega_{\text{constraint}}} d\Omega, \tag{4.13}$$

For an example, consider a previous parallelogram 4-electrode square model as shown <Fig. 2>. The B-spline function order for design variable parameterization is 8 and the constraint volume is 50%. <Fig. 19> shows

optimal shape and other results with initial model.

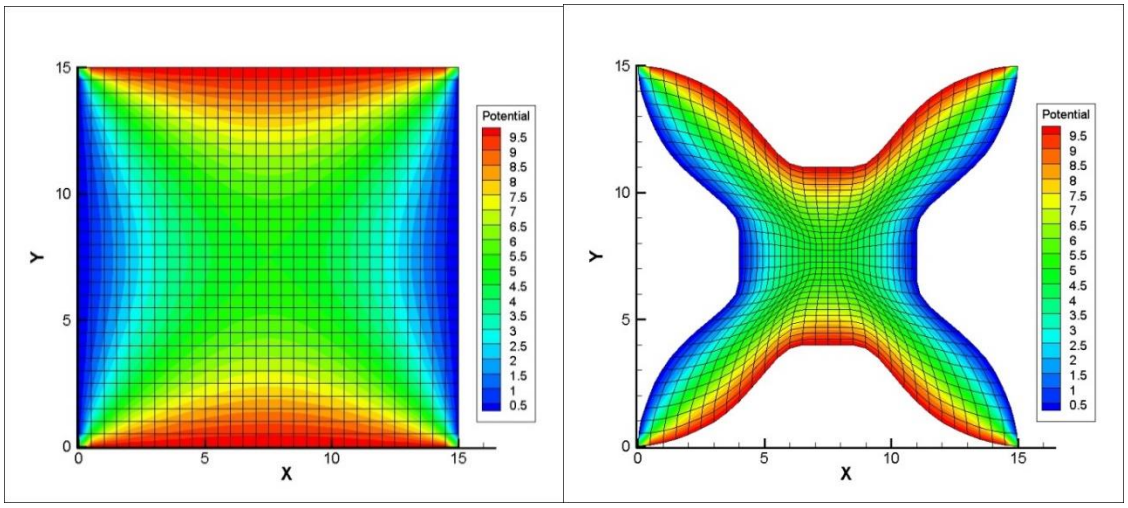

<Fig. 19 Shape optimization result: (a) initial model, (b) optimal model>

As shown in <Fig. 19>, it can be seen that the force of the DEP force tends to increase due to the concave shape of the central part. This is similar to the smooth quadratic curve obtained by assuming a polynomial function for the same example by Y. Huang [24]. Y. Huang analytically obtained the shape of the electrode that maximizes the dep force in the paper. In fact, this shape has been experimentally verified to maximize the DEP force. Therefore, it can be seen that the simulation results in this study agree with the known experimental results. <Fig. 20> shows the optimization history of the objective function. The objective function increased gradually for 5 iterations. It also implies the proposed method of shape optimization is effective.

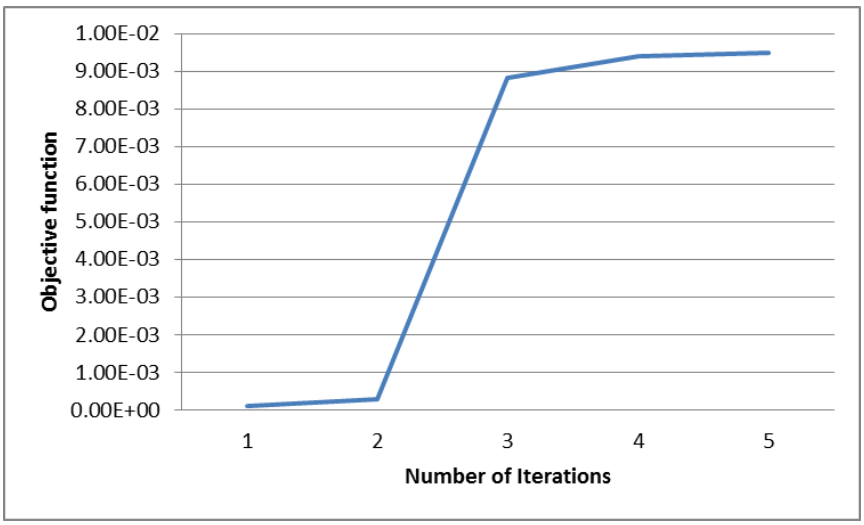

<Fig. 20 Shape optimization history>

5.3.4. Square-shaped electrode (DEP Force)

To proceed with the optimal design in a more complex geometry, consider the case where the initial geometry is curved. In general, it is known that the shape smoothly inward curved is close to the optimal shape for maximizing DEP Force[24]. Therefore, we investigate the influence of the shape of the electrode on the size of the DEP force by performing the optimization in the commonly known curved geometry. The initial geometry with proper curvature, which does not distort the mesh distribution, is made to be <Fig. 21-(a)> and optimization is performed shown in <Fig. 21-(b)>. The design velocity field is the same as in section 5.3.3 and the B-spline function order for design variable parameterization is 9 and the constraint volume is 50%.

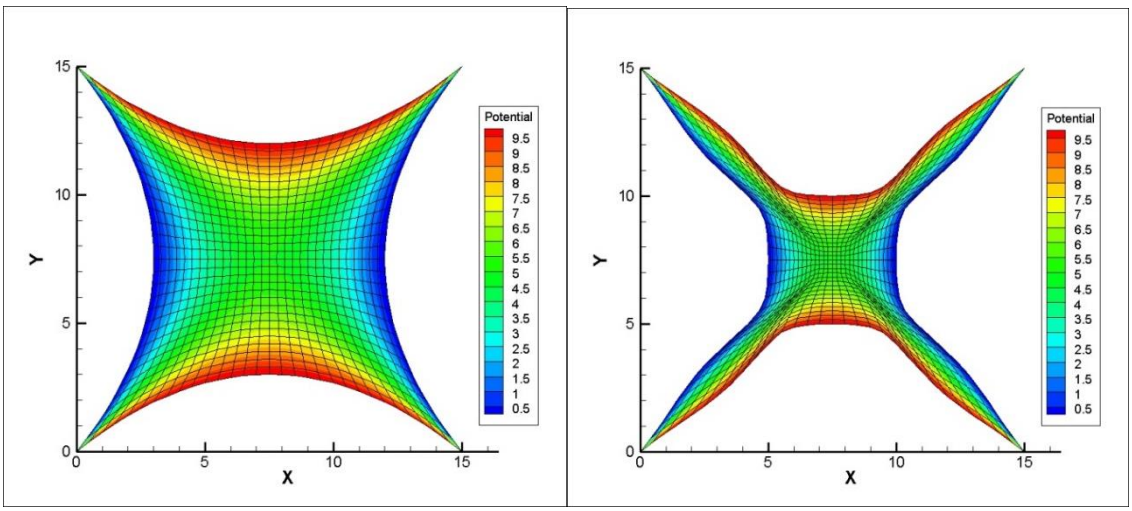

<Fig. 21 Shape optimization result: (a) initial model, (b) optimal model >

As can be seen in <Fig. 21>, an electrode shape that is more inward than a smooth curve which is obtained in Section 5.3.3. From this result, it can be seen that as the curve has more concave curvature inward, the magnitude of the DEP force increases. Therefore, if a higher magnitude of force is required to use the DEP force, it would be better to form the electric field by designing the center of the electrode more concave. The optimization history for this example is.

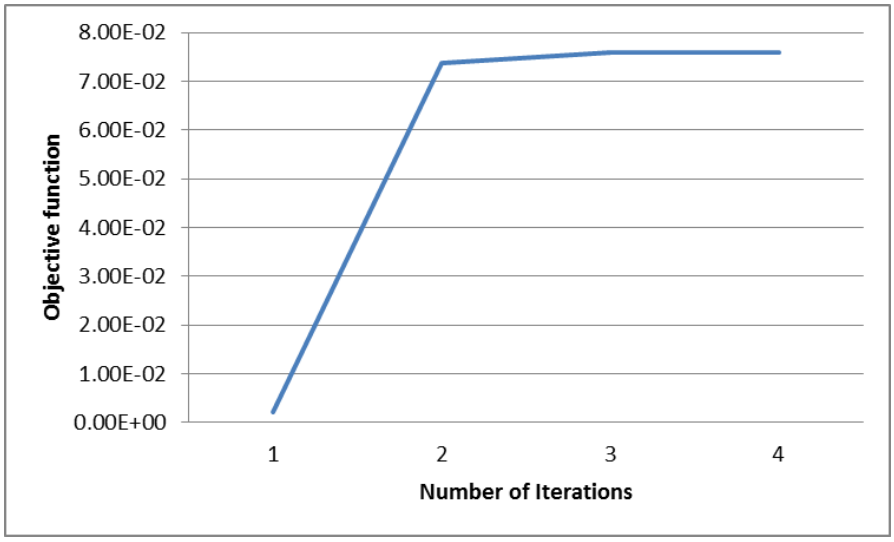

<Fig. 22 Shape optimization history>

As can be seen in <Fig. 22>, good convergence is obtained. DEP force is not

currently being actively studied in the shipbuilding marine engineering field, but it can be used in the post-treatment of ballast water as in previous studies[4] because DEP technology is highly applicable. The results of this study are expected to be used for exploration of DEP force in shipbuilding and marine engineering field.

5.4. Parametric study result for 3D electrodes

In this section, we performed parametric studies to determine the tendency of the total electric energy to change according to the shape of the electrode in the 3D situation. In 3D, an electric field is also formed in the direction of the thickness of the electrode, so that the same shape change may show a tendency opposite to that in 2D. Therefore, shape design optimization in 3D requires a much larger computation time and cost, so we make a simple parametric study using Comsol software to propose further study. As a reference model for parametric studies, we consider a basic model consisting of the following five parallel plates in <Fig. 23>.

In <Fig. 23>, the left figure shows the parallel plate model and the right figure shows actual electrode shape used for the electrolytic sterilization inside the ballast water tank of the ship. The parallel plate model is constructed by referring to the actual dimension of right electrode shape. According to IMO regulations, seawater in the ballast water tank must be discharged to the sea through a sterilization process[25]. One of the process is electrolytic sterilization method. The principle of sterilization using electrolysis is as follows. In the structure where the plates of the anode and the cathode cross each other, a complicated electric field is formed in the water tank. And the sea water in the water tank is strongly electrolyzed in proportion to the electric field strength. As a result of the electrolysis, HClO which sterilize the material is produced.

The faster the sterilization action in the ballast water tank, the lower the berthing time of the vessel. It means the higher utility of the economy. Since the volume of the electrode can also be considered as an economical cost, we can see that this problem is equivalent to the maximization of Total Electric Energy (TEE). Therefore, this problem model can be considered as a 2D extended electrostatic optimization problem which was discussed in section 5.3.3. The electrolytic water tank, which is produced and used in an actual industrial field, has a three-dimensional shape. Therefore, by observing the correlation between the TEE value and an element constituting the shape of the electrode, industrially useful results can be obtained.

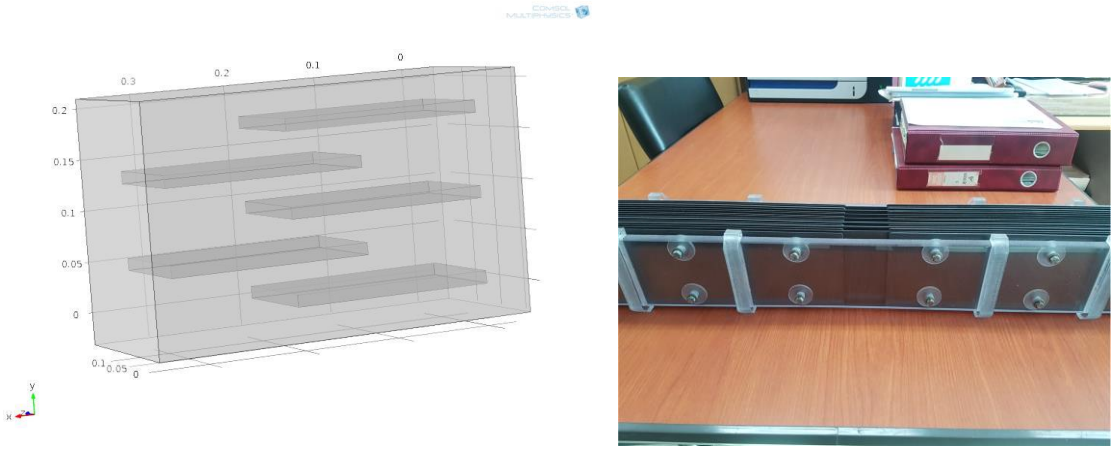

<Fig. 23 Basic parallel plate model>

The model is constructed as shown in <Fig. 23> and a potential of 200 V is applied to the odd-numbered plate from the top, and a potential of 0 V is applied to the other plates as shown in <Fig. 24>. In <Fig. 24>, the red part corresponds to the electric potential value of 200V and the blue part corresponds to the electric potential value of 0V. Since the electric field is a gradient of the electric potential as defined in Eq. (2.4), the yellow part which is rapidly changing from the red part to the blue part will be the strongest electric field intensity. Observing the distribution of the yellow part, it can be seen that the electric

field intensity is strong at the intersection of the anode and the cathode.

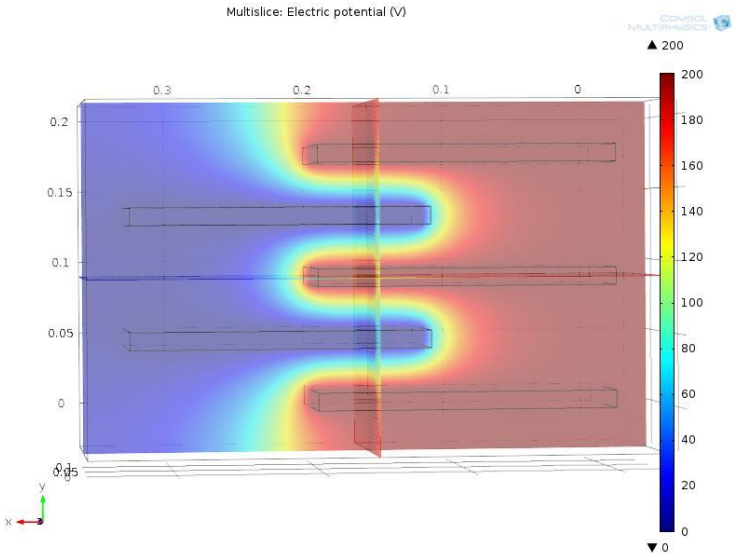

<Fig. 24 Electric field distribution>

The five parallel electrode plates are all of the same size. The dimensions of one electrode plate are as follows: width – 0.204 (m), depth – 0.012 (m), height – 0.11 (m) and the volume of one electrode is 0.000269. Using the internal analysis tool of Comsol software, we solve the electrostatic problem for the reference problem model and can obtain Total Electric Energy (TEE) value as shown in <Fig. 25>.

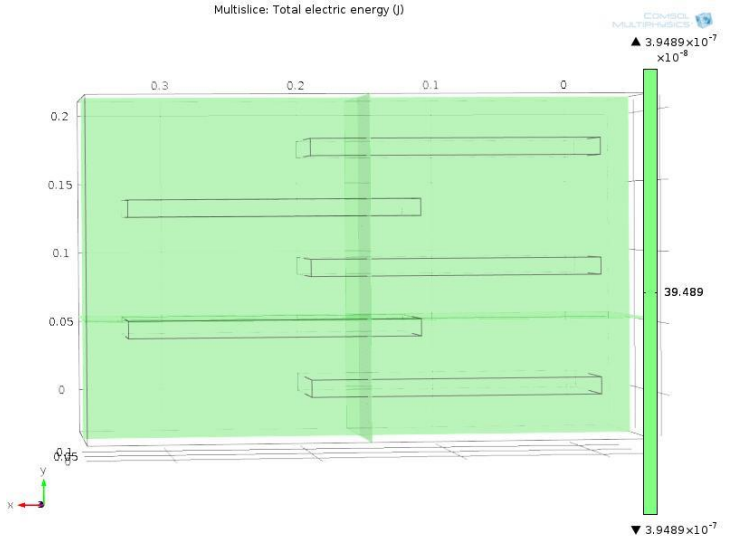

<Fig. 25 Total electric energy distribution>

As shown in <Fig. 25>, the TEE value of 3.9849E−07 is obtained in the basic parallel plate model. Our goal is to change the parameters (ex: width of electrode, height of electrode, distance between electrodes) that make up the reference model and study how the parameters affect the TEE value in the 3D environment. Using such a parametric study, we can explore the directionality of obtaining the optimal objective function in a given volume constraint. For the purpose of this study, we assumed the index of sensitivity to put the rate of change of volume as denominator with the rate of change of TEE as a numerator. The physical meaning of the indicator can be deduced from its definition. If the sensitivity value of a model is high, it means that the TEE value also varies significantly with small changes in the volume value. In terms of industry, the sensitivity index can be thought that the economic utility (TEE value) change due to economic cost (electrode volume) change. For an example, consider the following model which has perforated electrodes instead of original flat electrodes:

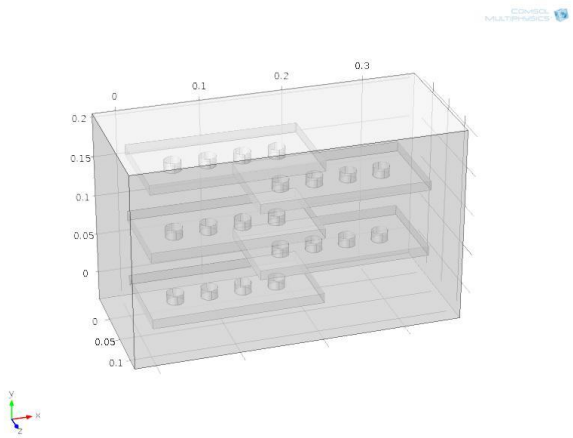

<Fig. 26 Example of a modified model>

The model shown in <Fig. 26> is a model where each plate with a radius of 0.01 (m) is placed at equal intervals of four holes in a basic parallel plate model.

By placing holes, the volume is lost by 1.51E−05 (m ^ 3). And as the electrode decreases in volume, TEE value decreased by −0.014E−07 for a plate. So, the volume change rate of the electrode for this example model is − (1.51E−05) / (0.000269) = 0.056058, and the TEE change rate is − (0.014) / (3.9489) = 0.003545. Therefore, the sensitivity index for this example model is (0.056058) / (0.003545) = 0.063243.

5.4.1. Creating holes in electrode

In this section, we will look at the tendency of changes in the sensitivity index to create holes in the electrodes. In the 2D environment, even if a hole is formed in the electrode, there is no change in the TEE value due to the reduction in the volume of the electrode. As shown in <Fig. 27>, since the same voltage is applied to the entire electrode, there is no change in the electric field distribution even if a crack is generated inside the electrode.

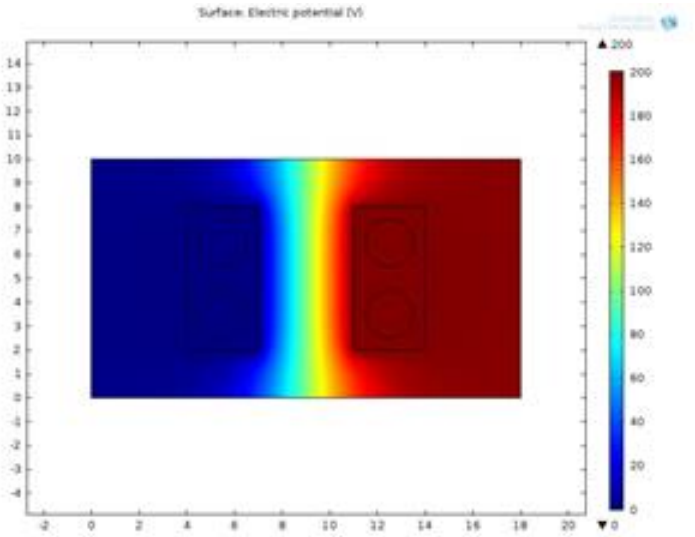

<Fig. 27 Electric voltage distribution with perforated electrodes in 2D environment>

This is a representative example that reveals the limitation of the 2d analysis which cannot consider the electric field distribution change in the electrode

thickness direction. Therefore, this parametric study examines how the TEE value changes when a hole is created in the electrode in 3d.

In this parametric study, the size and number of holes can be parameters that determine the shape of the electrode. Therefore, we try to study the change of TEE value by changing these factors little by little. We create one to five holes in the electrode and the generated holes were arranged at regular intervals. In addition to hole number change, the radius of the generated holes is divided into five types: 0.01 (m), 0.008 (m), 0.006 (m), 0.004 (m) and 0.002 (m). Therefore, we can make a problem model of 25 combinations with different numbers of holes and radius. This study aims to provide a clue to the 3D shape optimization by examining the change of the TEE sensitivity index of a total of 25(5x5) models. By changing the number of holes and the length of the radius, we can construct the following problem models <Fig. 28>.

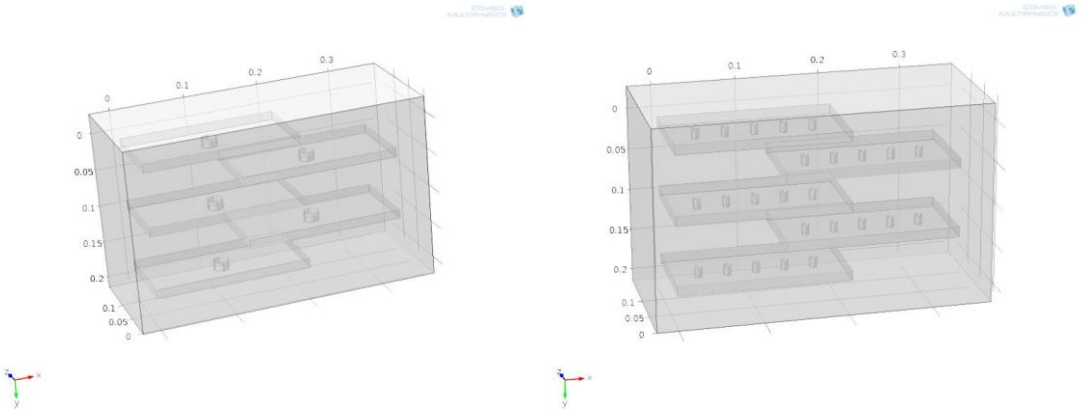

(a) (b)

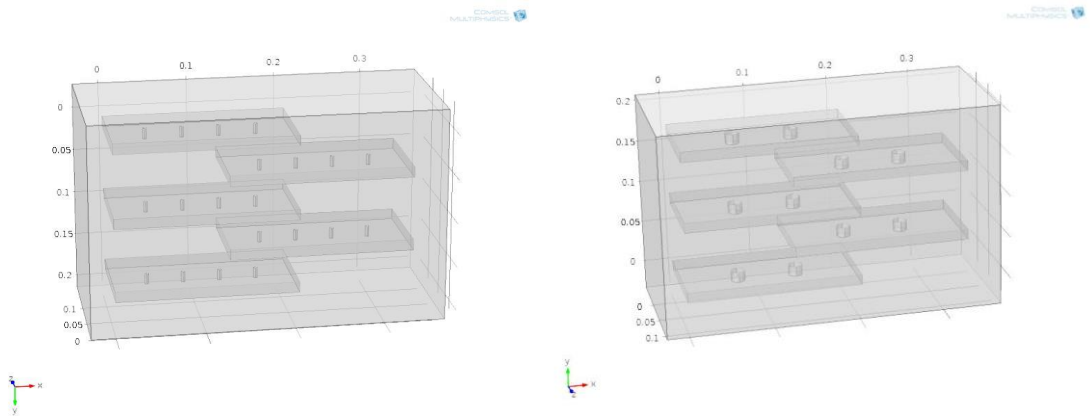

(c) (d)

<Fig. 28 Change of electrode shape due to change of radius in case of 1 hole>

<Fig. 28> shows four examples which are randomly extracted for understanding. <Fig. 28(a)> shows an electrode model with one hole whose radius is 0.01(m). <Fig. 28(b)> shows an electrode model with five holes whose radius is 0.004(m). <Fig. 28(c)> shows an electrode model with four holes whose radius is 0.002(m). <Fig. 28(d)> shows an electrode model with two holes whose radius is 0.008(m). As in the examples shown in <Fig. 28>, totally, 25 models can be constructed by varying the number and size of openings in the electrode. Detailed drawings of all 25 models are included in the appendix. The sensitivity index changes for 25 models are shown in the <Table 4> and <Fig. 29> as follows:

Number of hole	Radius	Sensitivity	Number of hole	Radius	Sensitivity
1	0.01	0.021683	3	0.006	0.031789
1	0.008	0.01694	3	0.004	0.015058
1	0.006	0.015058	3	0.002	−0.01506
1	0.004	−0.03388	4	0.01	0.063243
1	0.002	0.045174	4	0.008	0.047997

2	0.01	0.06776	4	0.006	0.035135
2	0.008	0.049409	4	0.004	0.028234
2	0.006	0.032625	4	0.002	0
2	0.004	0.011293	5	0.01	0.065773
2	0.002	−0.04517	5	0.008	0.05195
3	0.01	0.060834	5	0.006	0.03915
3	0.008	0.048938	5	0.004	0.024846
			5	0.002	0.009035

<Table 4 Sensitivity change according to the number and size of holes>

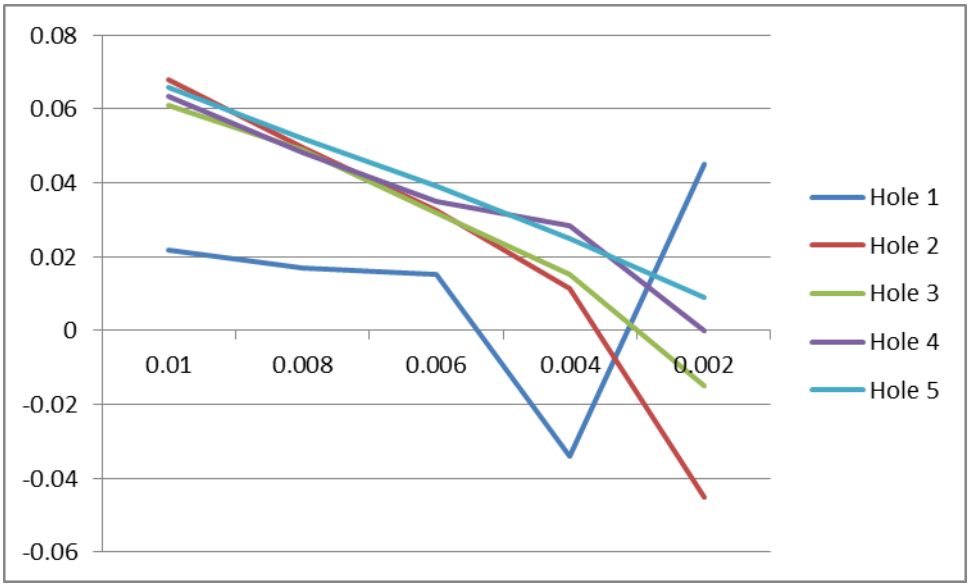

<Fig. 29 Sensitivity change according to the number and size of holes>

When referring to the above <Table 4>&<Fig. 29>, the overall tendency is that the smaller the radius, the smaller the sensitivity value. This parametric study is a case in which the volume of the electrode is lost. So, for this case, a small value of the sensitivity index means that the decrease in the TEE value is smaller than the decrease in the electrode volume. Therefore, we can conclude that if shape design optimization is performed by creating a hole in the electrode, it would be better to create small holes in the electrode.

If we compare the tendency of other data in <Fig. 29>, it can be deduced that the case of Hole 1 shows distorted tendency due to errors in model setting. Considering that the electric energy is usually generated at the edge of the plate, the fact that only one hole is placed at the edge of the plate is considered to be the main cause of the different tendency. In addition, when the radius of the hole is the smallest at 0.002, the sensitivity index tends to fall to a negative value. If the sensitivity index has a negative value, this means that the TEE value has increased as the volume of the electrode decreases. This is a physically difficult phenomenon. Therefore, considering that the size of the sensitivity indicator is very small in this case, it can be deduced that a negative value is obtained due to the numerical error.

5.4.2. Changing the position of a hole in the electrode

In this parametric study, we examine the change of the TEE value with respect to the positional change of the hole created in the electrode. This study can have a great academic significance in connection with the previous research. In association with the result of the change in the TEE value for the number of holes studied in the preceding parametric study, it is possible to effectively determine the number of holes at any position on the electrode surface in achieving the target TEE value,

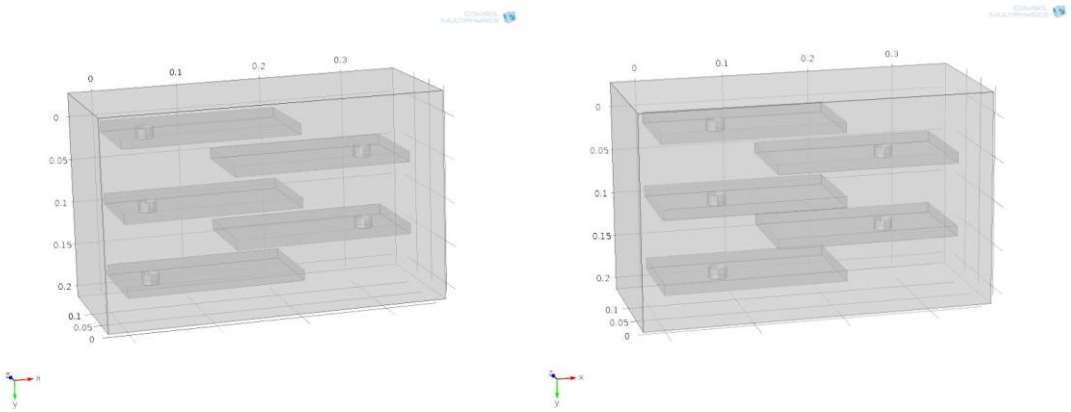

<Fig. 30 Change of electrode shape with change of hole position: Model 1&2>

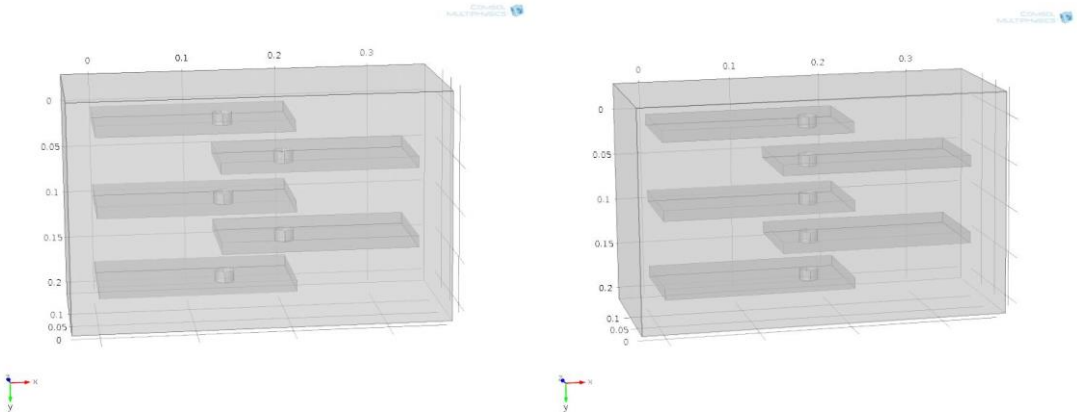

<Fig. 31 Change of electrode shape with change of hole position: Model 3&4>

The problem model is constructed by changing the position of a circle with a radius of 0.01 (m) in the basic parallel plate model as shown in above <Fig. 30-31>. In <Fig. 10-11>, the model on the upper left is the case where the hole is farthest from the intersection of the electrodes, and the hole gradually moves to the intersection of the electrodes and becomes the model of the lower right. The change in sensitivity index for the model change is shown in the following graph.

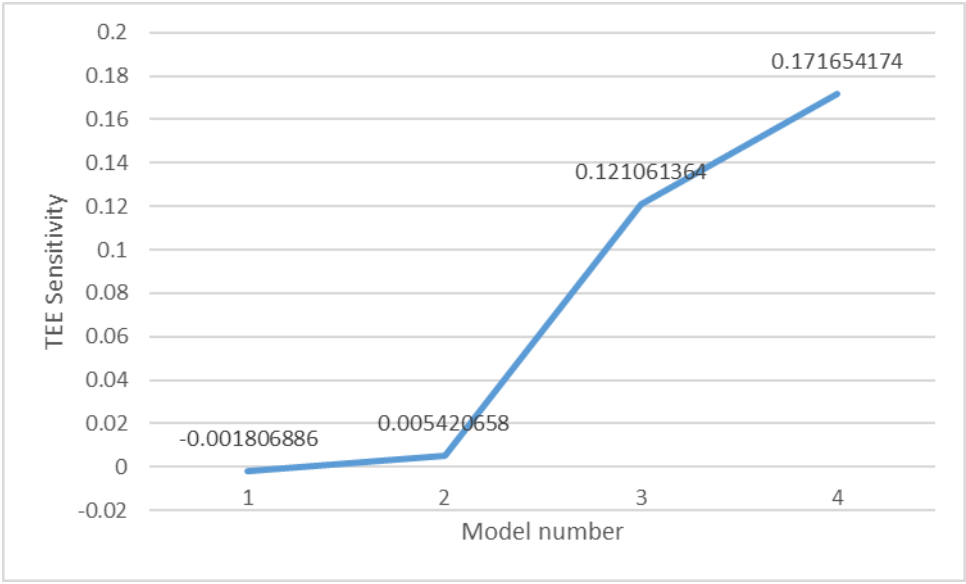

<Fig. 32 Change of sensitivity value for position change of electrode hole >

<Fig. 32> shows the change in sensitivity value for the change of the position of the electrode hole. Overall, the sensitivity changes from model 1 to model 4, indicating a tendency to increase sensitivity. This means that the TEE value changes sensitively when the position of the hole created in the electrode is generated near the intersection of the electrodes. In this parametric study, the volume of the electrode decreased. Therefore, the loss rate of TEE decreases as the position of the generated hole is farther from the intersection of the electrodes. Thus, creating a hole in an electrode will produce greater electrical energy if the electrode is created far from the intersection.

5.4.3. Forming grooves in the electrode

In this parametric study, the groove was formed on the side of the electrode and the change of the TEE value according to the shape of the electrode was observed. Creating grooves in the electrode is a change that affects the roughness of the electrode surface. If there are many grooves or deep in the electrode surface, it will have the effect of making the surface rougher. Conversely, if there is a small or shallow groove on the surface of the electrode, the surface will produce an effect similar to a smooth electrode. Therefore, this parametric study is to investigate the correlation between the surface roughness and the TEE value. In this study, the depth, thickness, and number of grooves were changed in some steps and the change of TEE value was examined. By changing those parameters, we can construct the following problem models in <Fig. 33−35>.

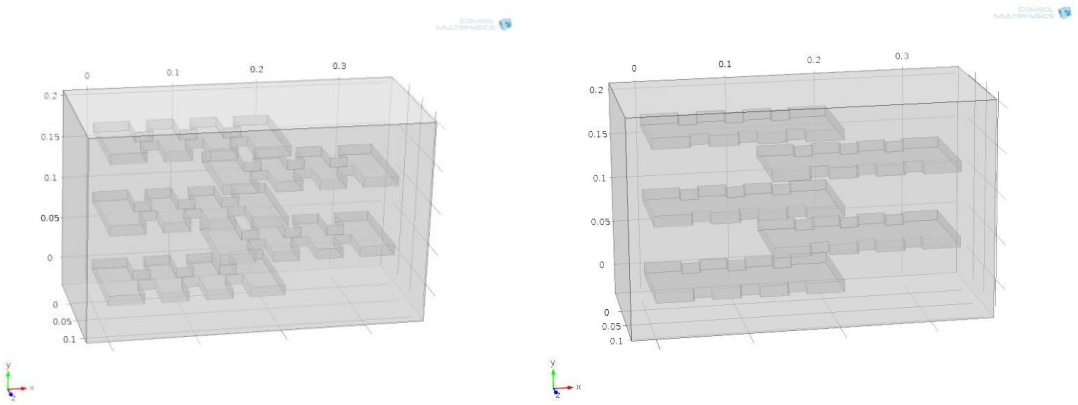

<Fig. 33 Change of shape according to depth of electrode groove>

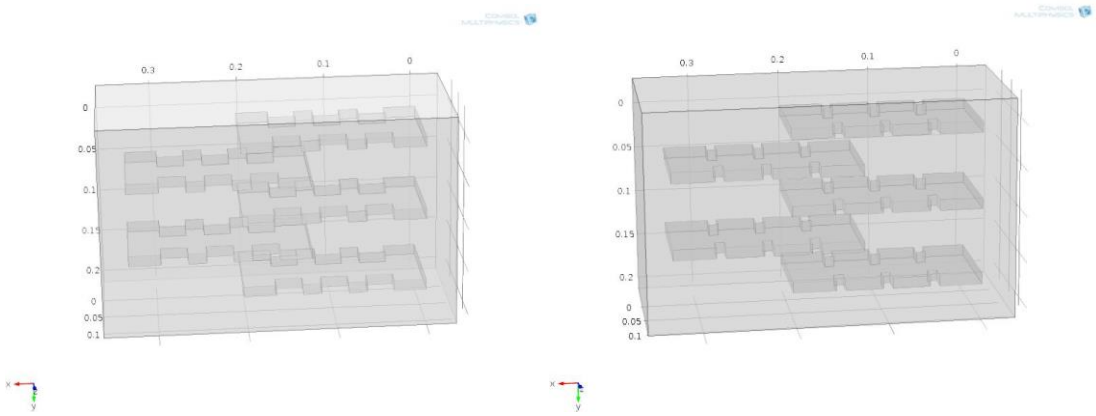

<Fig. 34 Change of shape according to width of electrode groove>

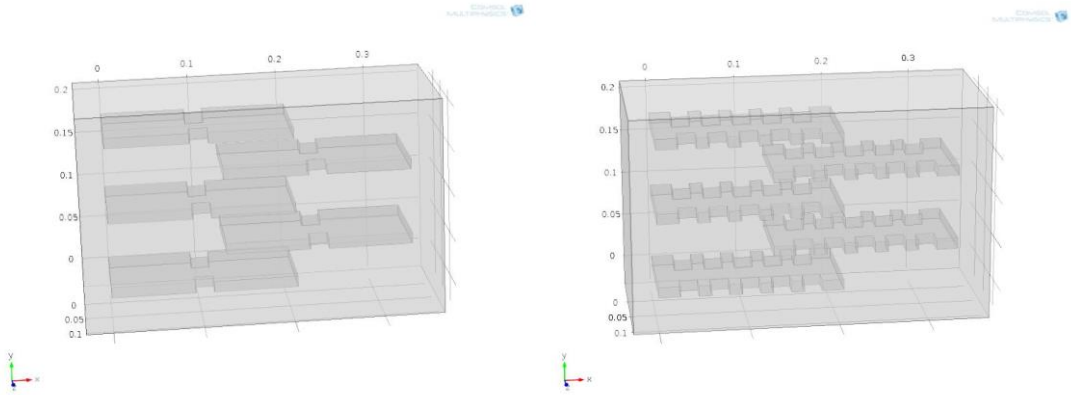

<Fig. 35 Change of shape according to number of electrode groove>

The above <Fig. 33-35> shows how each parameter changes in some way through two representative examples. <Fig. 33> shows two problem models

with varying groove depths under the same number and width. <Fig. 34> shows two problem models with varying groove widths under the same number and depth. <Fig. 35> shows two problem models with varying groove numbers under the same depth and width. The graph of the sensitivity index change is as follows. (Detailed drawings of other problem models are included in the appendix).

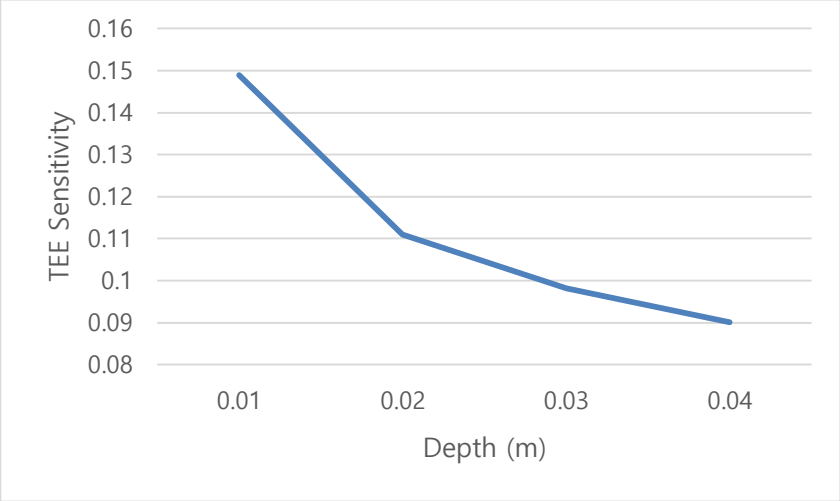

<Fig. 36 Change of sensitivity value for depth change of grooves >

<Fig. 36> shows the change in sensitivity value for the change of depth of the grooves in the electrode. Overall, as depth increases, TEE sensitivity decreases. It also implies that the TEE value changes sensitively When the depth of the groove is small. In this parametric study, the volume of the electrode decreased. Therefore, as the depth of the generated groove is deepened, the loss rate of TEE decreases.

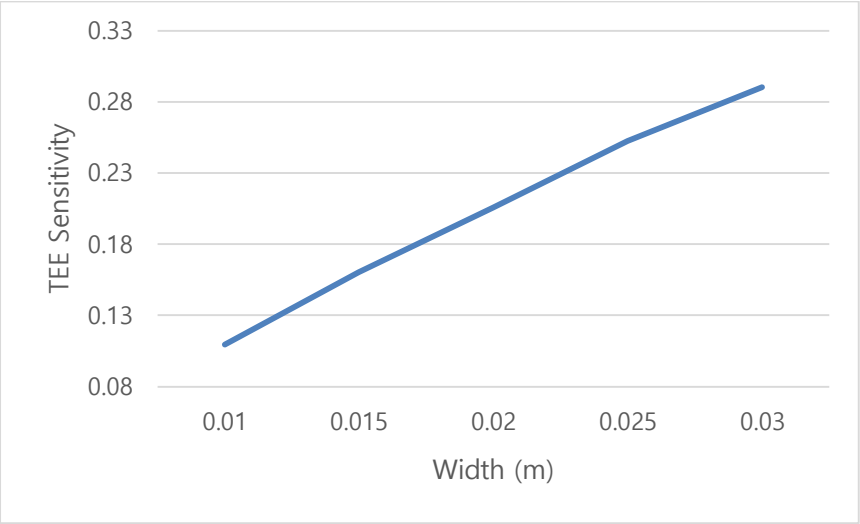

<Fig. 37 Change of sensitivity value for width change of grooves >

<Fig. 37> shows the change in sensitivity value for the change of width of the grooves in the electrode. Overall, as width increases, TEE sensitivity increases. It also implies that the TEE value changes sensitively When the width of the groove is large. In this parametric study, the volume of the electrode decreased. Therefore, as the width of the generated groove is smaller, the loss rate of TEE decreases.

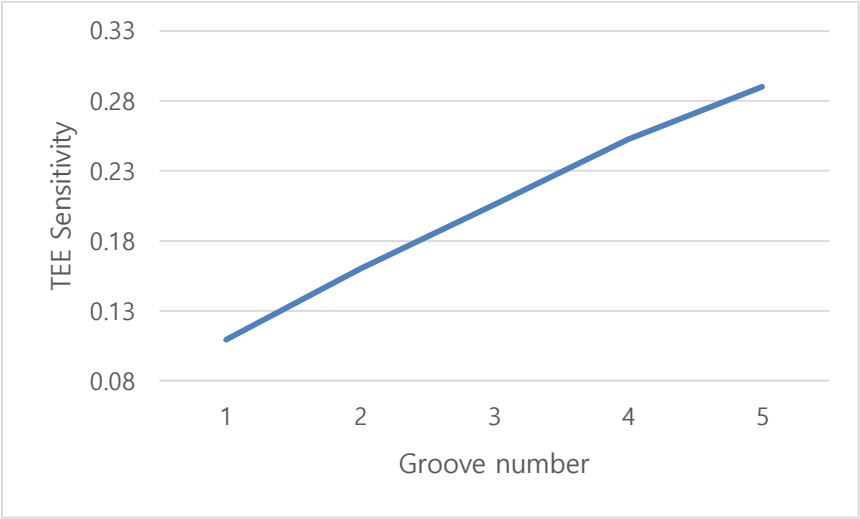

<Fig. 38 Change of sensitivity value for number change of grooves >

<Fig. 38> shows the change in sensitivity value for the change of number of

the grooves in the electrode. Overall, as number increases, TEE sensitivity increases. It also implies that the TEE value changes sensitively When the number of the groove is high. In this parametric study, the volume of the electrode decreased. Therefore, as the number of the generated groove is smaller, the loss rate of TEE decreases.

6. Conclusion

Using the finite element method and the efficient adjoint DSA method, a shape sensitivity analysis is derived for electrostatic problems in a steady state. In the FEM-based approach, it is possible to vary the boundary of a structure by directly placing the position of the nodal points for the design variables. In the FEM-based shape optimization, the shape of the boundary is wiggled due to many design variables, so the mesh quality is degraded at every optimization iteration. To solve this problem, design variables were parameterized by B-spline function and minimized Dirichlet energy function for every optimization iteration to maintain high mesh quality. Since the sensitivity of an analytically derived electrostatic problem is applied to an optimization algorithm, it can be seen that a convergence history is observed in which the objective function gradually increases in various examples. Through shape optimization research, we have obtained an optimal electrode shape that produces an electric field distribution. The achievement of this research will help to produce electrodes for the purpose of future research. A parametric study was conducted to investigate the effect of the shape change of the electrode in the 3D environment. In a situation where the electrical energy needs to be maximized as in the ballast water tank of a ship, it would be cost effective to use an electrode with the following conditions: 1) the surface hole size is small, 2) porous, 3) the surface

is rough. In this 3d environment parametric study, the tendency was limited to the square model like the ballast water tank of the ship, but the study of the electrode shape change or other objective function can be further studied

References

[1] H.A. Pohl, Dielectrophoresis: The Behavior of Neutral Matter in Non-uniform Electric Fields, Cambridge University Press, Cambridge, UK, 1978.

[2] Gascoyne, P.R.C., Vykoukal, J., Particle separation by dielectrophoresis, Electrophoresis 23 (13) (2002) pp. 1973-1983.

[3] Voldman, J., Electrical forces for microscale cell manipulation, Annual Review of Biomedical Engineering 8 (2006) pp. 425-454.

[4] Wang Y, Wang J, Wu X, Jiang Z, Wang W., Dielectrophoretic separation of microalgae cells in ballast water in a microfluidic chip, Electrophoresis 40 (6) (2018) pp. 969-978.

[5] Lapizco-Encinas, B.H., Davalos, R.V., Simmons, B.A., Cummings, E.B., Fintschenko, Y., An insulator-based (electrodeless) dielectrophoretic concentrator for microbes in water, Journal of Microbiological Methods 62 (3 SPEC. ISS.) (2005) pp. 317-326.

[6] Lapizco-Encinas, B.H., Simmons, B.A., Cummings, E.B., Fintschenko, Y., Dielectrophoretic Concentration and Separation of Live and Dead Bacteria in an Array of Insulators, Analytical Chemistry 76 (6) (2004) pp. 1571-1579.

[7] Tegenfeldt, J.O., Prinz, C., Cao, H., Huang, R.L., Austin, R.H., Chou, S.Y., Cox, E.C., Sturm, J.C., Micro- and nanofluidics for DNA analysis, Analytical and

Bioanalytical Chemistry 378 (7) (2004) pp. 1678-1692.

[8] M.-B. Shon, M.H. Son, J. Lee, Y.-J. Son, G.H. Lee, C.H. Moon and Y.-S. Kim., The Study on the Marine Eco-toxicity and Ecological Risk of Treated Discharge Water from Ballast Water Management System Using Electrolysis, Journal of the Korean Society for Marine Environment and Energy 16 (2) (2013) pp. 88-101.

[9] Og-Yeol Bag.Jang Moon.Jun-Mo Park, Gil-Young Kon., Development of the Electrolysis Ballast Water Treatment System and Test, J . Navig. P ort Res. 41 (3) (2017) pp. 79-86.

[10] Yoon, G.H., Park, J., Topological design of electrode shapes for dielectrophoresis based devices, Journal of Electrostatics 68 (6) (2010) pp. 475-486.

[11] J. Park, B.Kim, S.K.Choi, S.Hong, S.H. Lee, K.I. Lee, An efficient cell separation system using 3D-asymmetric microelectrodes, Lab on a Chip 5 (2005) pp. 1264-1270.

[12] Kinio, S. & Mills, J.K., Design of optimal electrode geometries for dielectrophoresis
using fitness based on simplified particle trajectories, Biomed Microdevices (2016) 18: 69.

[13] Sigmund, O. & Petersson, J., Numerical instabilities in topology optimization: A survey on procedures dealing with checkerboards, mesh-dependencies and local minima, Structural Optimization 16 (1998), pp. 68-75.

[14] Braibant V and Fluery C., Shape optimal design using B-splines, Computer Methods in Applied Mechchanics and Engineering 44 (1984), pp. 247-267.

[15] Azegami H, Kaizu S, Shimoda M, et al., Irregularity of shape optimization problems and an improvement technique, Computer Aided Optimum Design Structures V (1997), pp. 309–326.

[16] T.M. Yao, K.K. Choi, 3–D shape optimal design and automatic finite element regridding, International Journal for Numerical Methods in Engineering 28 (1989), pp. 369–384.

[17] S.Y. Hsu, C.L. Chang, Mesh deformation based on fully stressed design: the method and 2–D examples, International Journal for Numerical Methods in Engineering 72 (2007), pp. 606–629.

[18] X. Wang, X. Qian, An optimization approach for constructing trivariate B–spline solids, Computer Aided Design 46 (2014), pp. 179–191.

[19] Gang Xu, Bernard Mourrain, R´egis Duvigneau, Andr´e Galligo, Constructing analysis–suitable parameterization of computational domain from CAD boundary by variational harmonic method, Journal of Computational Physics 252 (1) (2013), pp. 275–289.

[20] Myung–Jin Choi, Seonho Cho, A mesh regularization scheme to update internal control points for isogeometric shape design optimization, Computer Methods in Applied Mechanics and Engineering Volume 285 (2015), pp. 694–713.

[21] Klaus–Jurgen Bathe, Finite Element Procedures 2nd Edition, Prentice Hall, Pearson Education, Inc, 2014.

[22] E.J.Haug, K.K.Choi , V.Komkov, Design Sensitivity Analysis of Structural Systems, Academic, New York, 1986.

[23] M.S. Floater, K. Hormann, Surface parameterization: a tutorial and survey,

in: N.A. Dodgson, M.S. Floater, M.A. Sabin (Eds.), Advances in Multiresolution for Geometric Modelling, Springer-Verlag, Heidelberg, 2005, pp. 157-186.

[24] Y Huang, R pethig, Electrode design for negative dielectrophoresis, Measurement Science and Technology, Volume 2, Number 12 (1991), pp. 1142-1146.

[25] IMO, BWM Convention / Section B-1 : IMO, 2017.

Abstract

Shape design optimization

of electrostatic problems

Jeong Hong Yeon

Dept. of Naval Architecture & Ocean Enginnering

The Graduate School

Seoul National University

The electric field generated by the electrode can be applied in various fields in engineering. In the shipbuilding marine engineering field, electric field analysis is carried out in the process of disinfecting ship ballast water. IMO regulations have made regulations on the quality of ballast water discharged to the oceans more stringent. Therefore, there has been actively studied an electrolysis method capable of sterilizing the ballast water simply and effectively. In order to conduct research in this direction, it is necessary to observe how the shape change of the electrode changes the electric field. It is also possible to find an optimal electrode shape from the tendency.

From the governing equation of the electrostatic problem, a weak form for finite element analysis was derived. And from that equation, a continuum-based design sensitivity analysis (DSA) method is developed for electrostatic problem. To consider high order objective function, we use 9-node FEM basis function for analysis and DSA method. Specifying design variables in shape optimization is an important issue. If there are too many design variables, it is likely to result in an optimal shape that cannot be produced. Since design variables are parameterized with B-spline function, we can obtain smooth boundary variations. In addition, the mesh quality may drop sharply due to the shape change of the structure during optimization. To solve mesh entanglement problem in optimization process, mesh regularization scheme is used. By minimizing Dirichlet energy functional, mesh uniformity can be automatically obtained.

For verifying our numerical simulation, numerical examples are compared with Comsol software results. The analysis results will be verified by comparison with the Comsol software results, and the change in the sensitivity value will be verified by the Finite Difference Method. The obtained optimal electrode geometry characteristics and optimization histories are specifically discussed. Finally, for the further study, an electrode shape parametric study was performed in 3D environment. This is because optimization in 3D requires too much computation cost to proceed with the simulation. Based on the results obtained through the parametric study, the orientation of electrode shape optimization in the 3D environment is presented.

Keywords: Electrostatic, Shape design sensitivity, Optimal electrode geometry, Mesh regularization, Comsol software, 3D parametric study

Student Number: 2016-21140

Appendix

A.

The figures at the bottom represent 25 models that were interpreted as problem models in section 5.4.1.

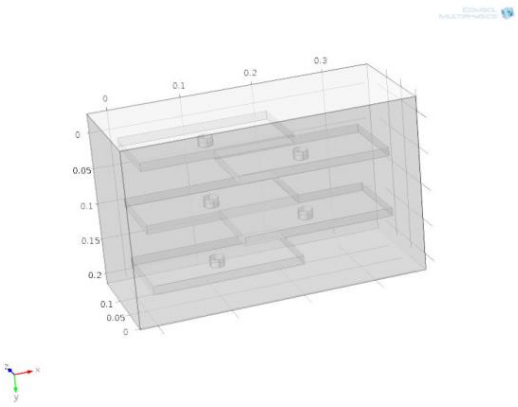

Radius: 0.01 (m)

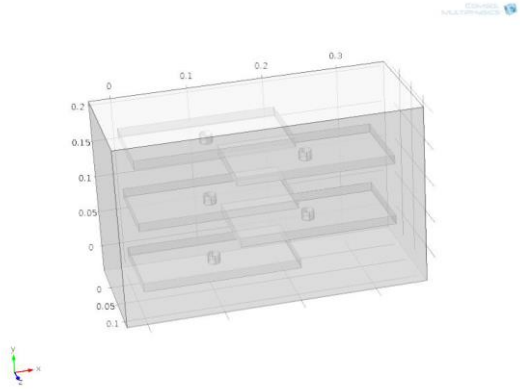

Radius: 0.008 (m)

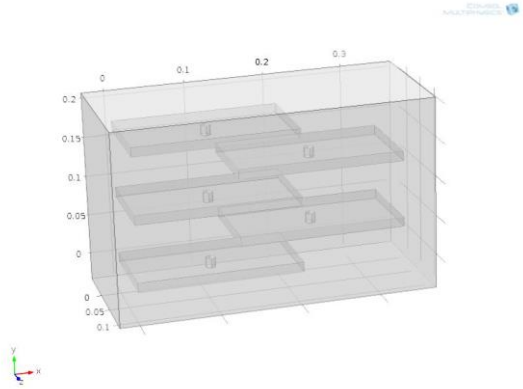

Radius: 0.006 (m)

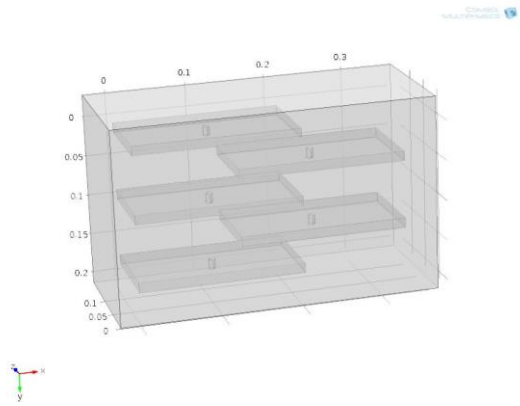

Radius: 0.004 (m)

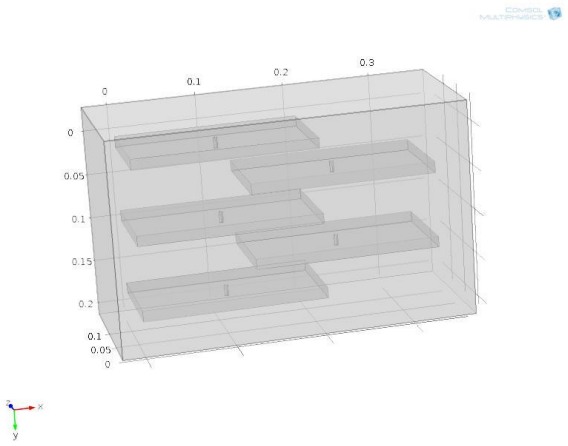

Radius: 0.002 (m)

<**Fig. 1** Model shape change of electrode shape due to change of radius in case of 1 hole>

<Fig. 1> shows a model created by creating only one hole in the electrode and slightly reducing the hole radius. Since the position of the hole is distributed equally on the electrode, the hole is located at the center in this case. <Fig. 2-5> shows the problem models by varying the number of holes to be created and decreasing the size of the radius as in <Fig. 1>.

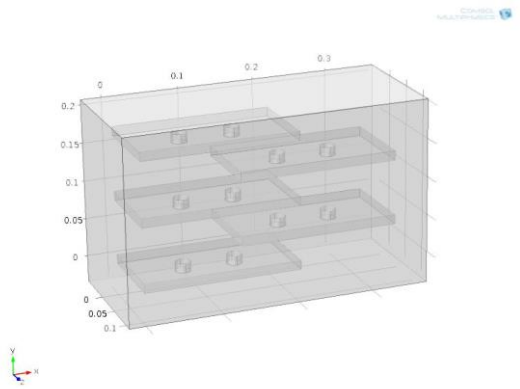

Radius: 0.01(m)

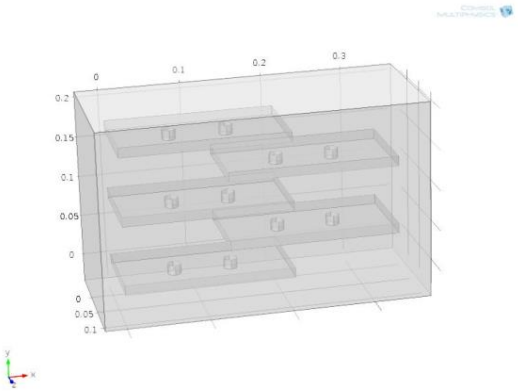

Radius: 0.008(m)

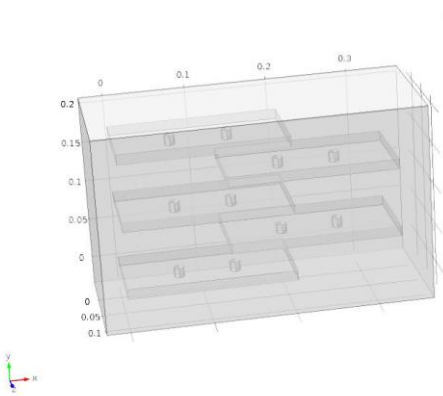

Radius: 0.006(m)

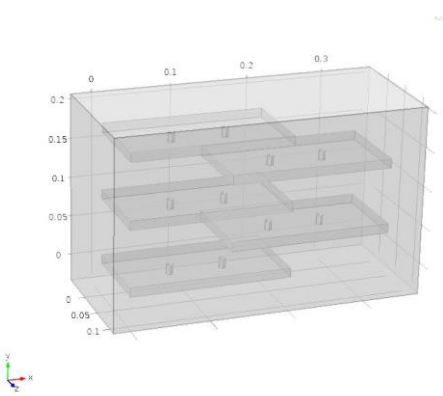

Radius: 0.004(m)

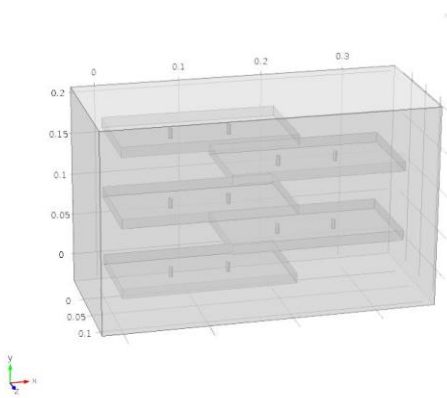

Radius: 0.002(m)

<Fig. 2 Model shape change of electrode shape due to change of radius in case of 2 hole>

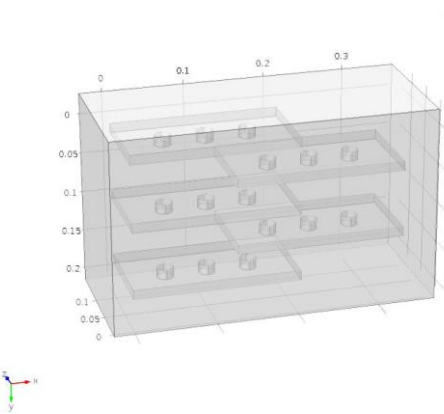

Radius: 0.01(m)

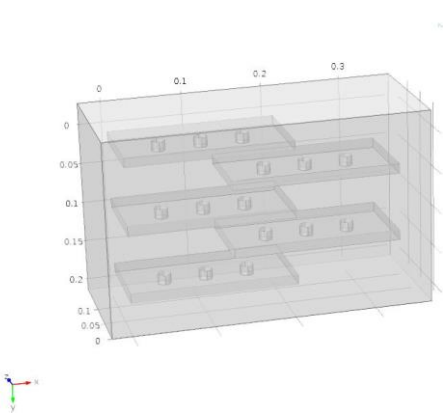

Radius: 0.008 (m)

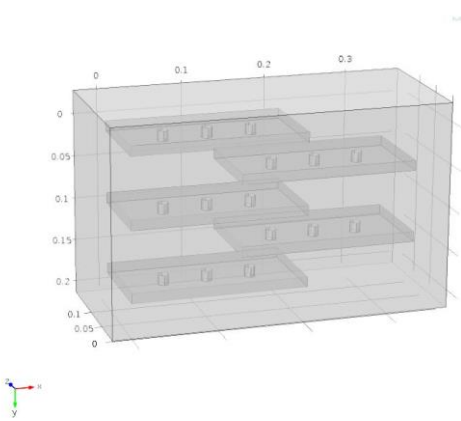

Radius: 0.006(m)

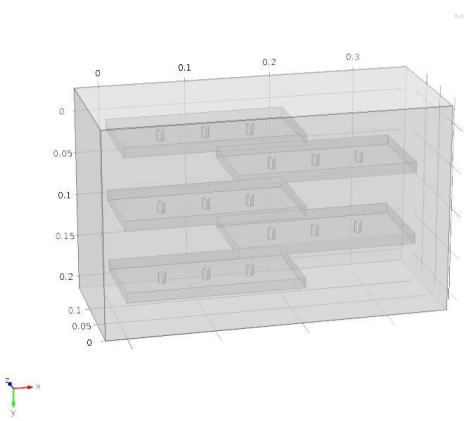

Radius: 0.004(m)

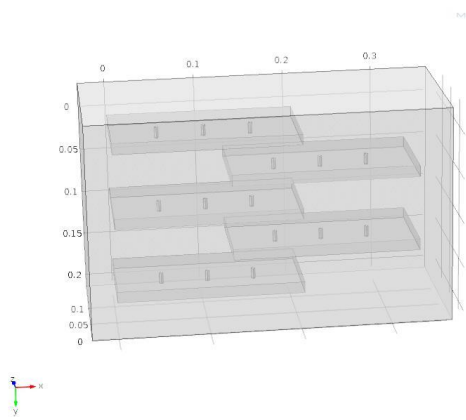

Radius: 0.002(m)

<Fig. 3 Model shape change of electrode shape due to change of radius in case of 3 hole>

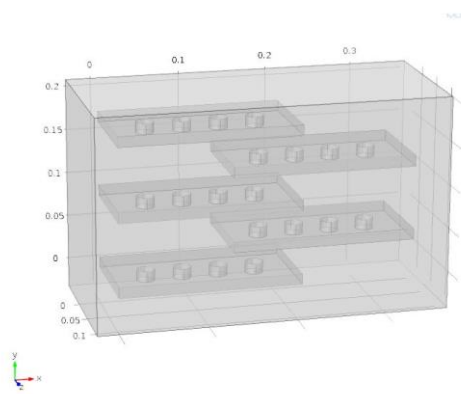

Radius: 0.01(m)

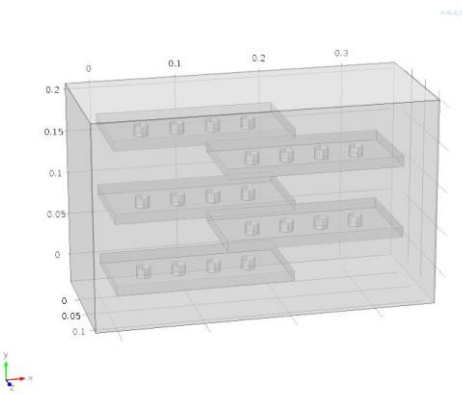

Radius: 0.008(m)

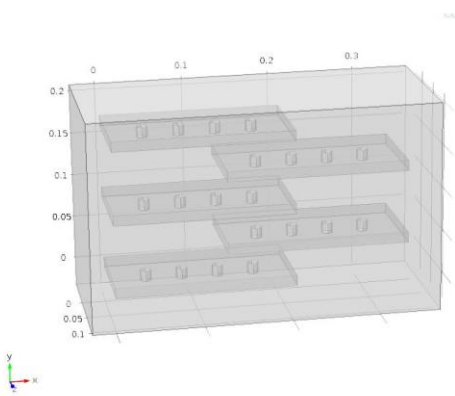

Radius: 0.006(m)

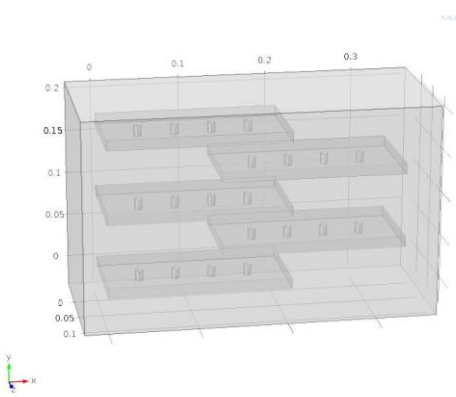

Radius: 0.004(m)

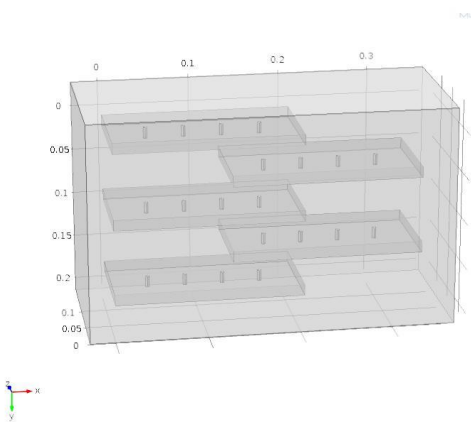

Radius: 0.002(m)

<Fig. 4 Model shape change of electrode shape due to change of radius in case of 4 hole>

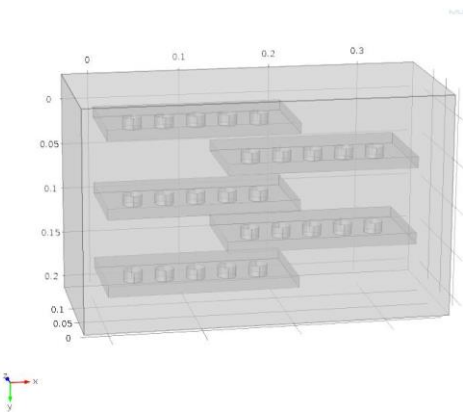

Radius: 0.01(m)

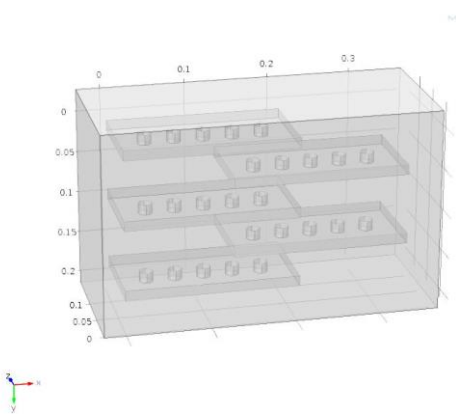

Radius: 0.008(m)

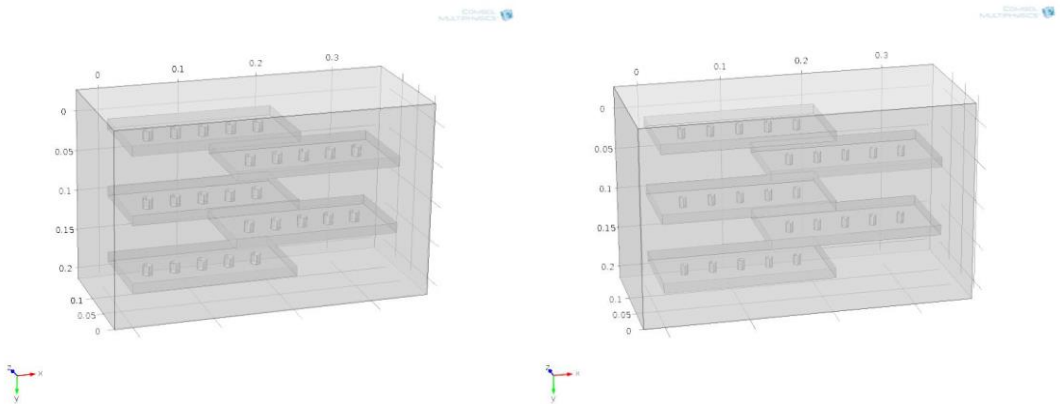

Radius: 0.006(m)　　Radius: 0.004(m)

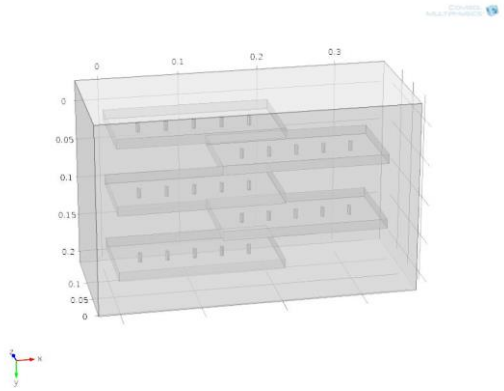

Radius: 0.002(m)

<Fig. 5 Model shape change of electrode shape due to change of radius in case of 5 hole>

As can be seen in <Fig. 1−5>, all of the holes are generated at equal intervals, and there are no variables other than the number of holes and the size of the radius. Therefore, if we examine the change of TEE value through the analysis of the above 25 models, we can deduce the tendency of TEE value change according to the number and size of holes created in the electrode.

B.

<Fig. 6-8> at the bottom shows a detailed figure of the entire example models that have some grooves in the electrode in section 5.4.3.

B.1. Problem models with varying groove depths

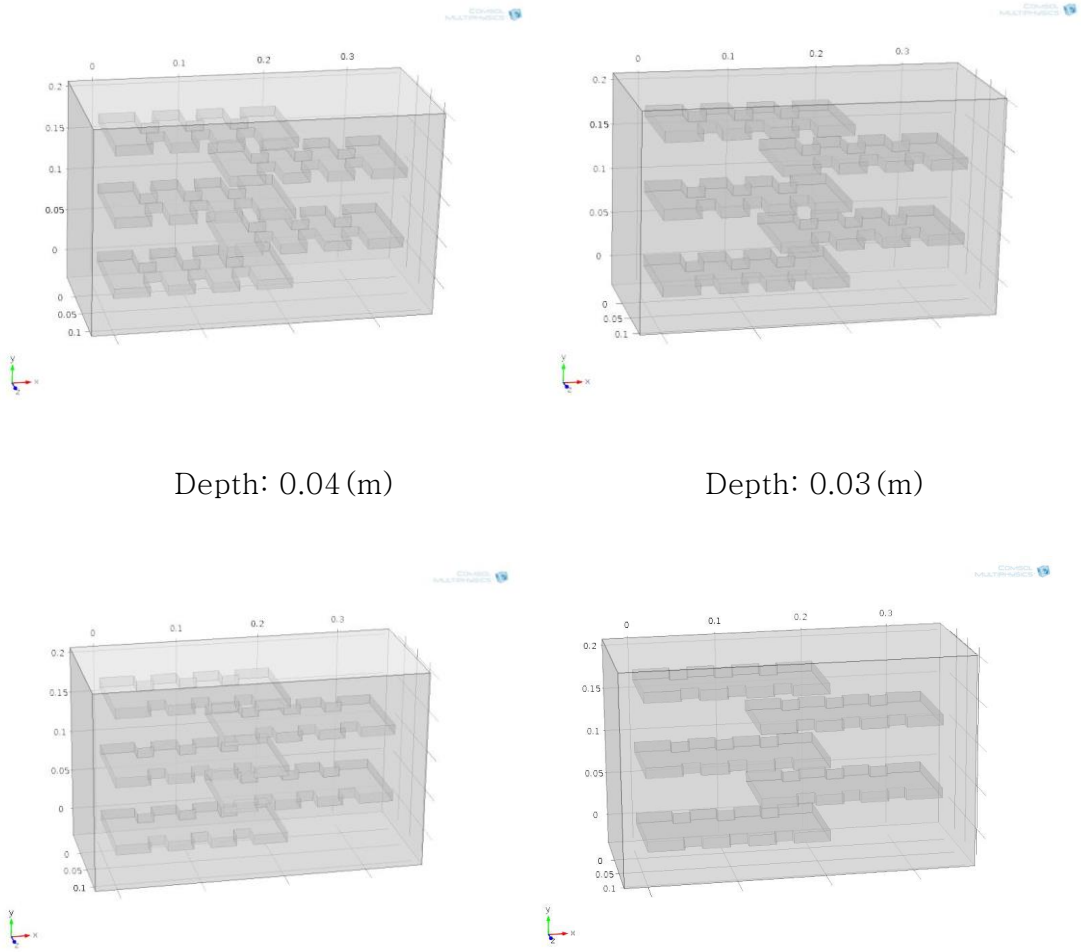

Depth: 0.04(m) Depth: 0.03(m)

Depth: 0.02(m) Depth: 0.01(m)

<Fig. 6 Model shape change of shape according to depth of electrode groove>

<Fig. 6> shows the change of electrode shape according to the depth of electrode groove. The width and number of the electrodes were kept the same, and only the depth of the electrode was changed. As the depth of the groove increases, the roughness of the electrode increases. Therefore, the potential value changes abruptly on the surface, resulting in a high electric

field distribution.

B.2. Problem models with varying groove widths

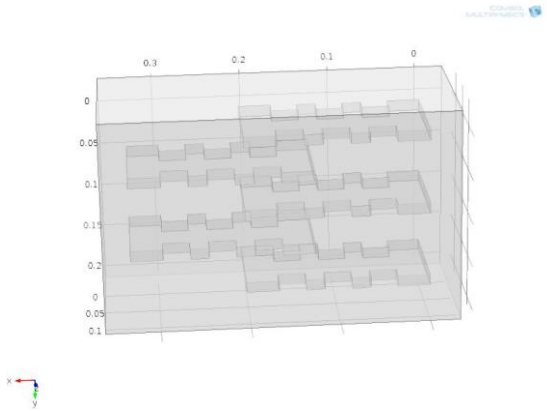

Width: 0.03(m)

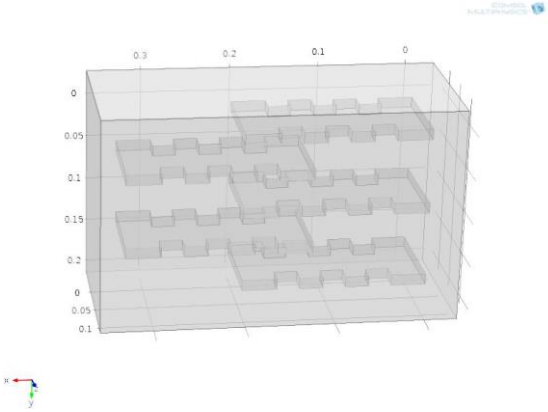

Width: 0.025(m)

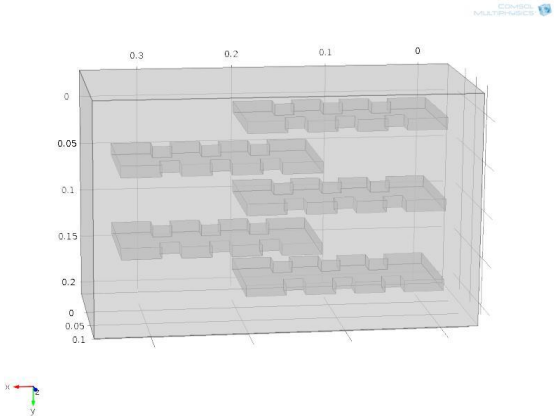

Width: 0.02(m)

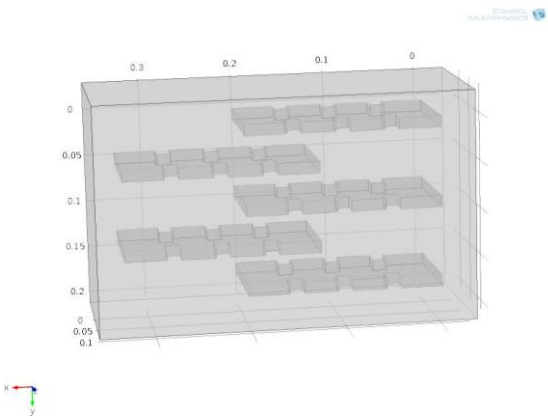

Width: 0.015(m)

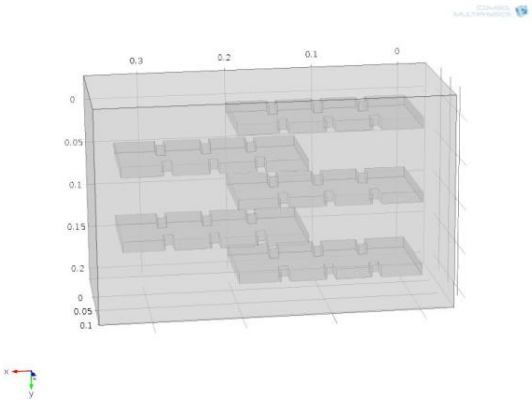

Width: 0.01(m)

<Fig. 7 Model shape change of shape according to width of electrode groove>

<Fig. 7> shows the change of electrode shape according to the width of electrode groove. The number and depth of the electrodes were kept the same, and only the width of the electrode was changed. As the width of the groove decreases, the shape of the electrode surface changes abruptly. Therefore, the potential value changes abruptly on the surface, resulting in a high electric field distribution.

B.3. Problem models with varying groove numbers

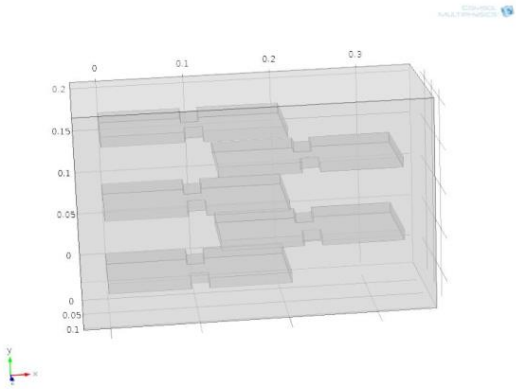

Groove number: 1

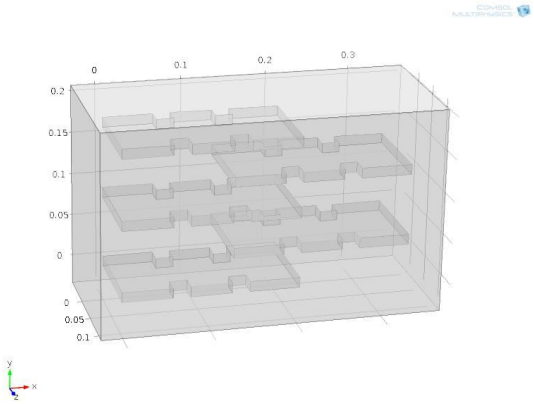

Groove number: 2

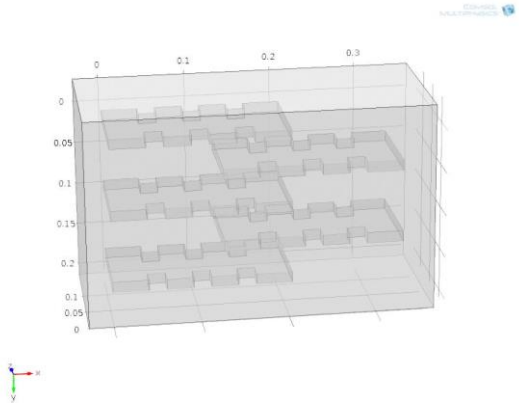

Groove number: 3

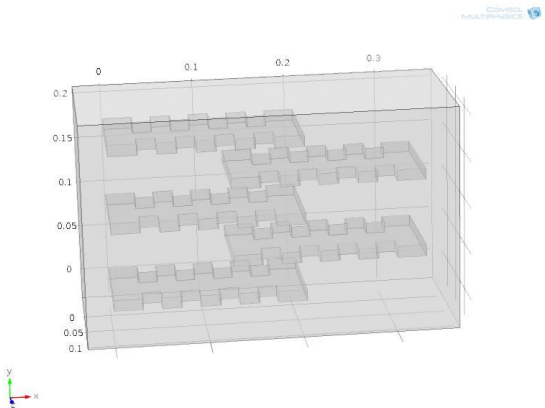

Groove number: 4

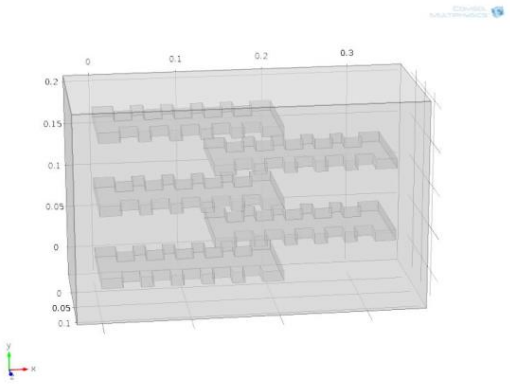

Groove number: 5

<Fig. 8 Change of shape according to number of electrode groove>

This parametric study also shows similar results to previous studies. <Fig. 8> shows the change of electrode shape according to the number of electrode groove. The width and depth of the electrodes were kept the same, and only the number of the electrode was changed. As the number of the groove increases, the shape of the electrode surface changes abruptly. Therefore, the potential value changes abruptly on the surface, resulting in a high electric field distribution.